REAL-TIME MONITORING OF POWDER MASS FLOWRATES FOR MPC/PID CONTROL OF A CONTINUOUS DIRECT COMPACTION TABLET MANUFACTURING PROCESS
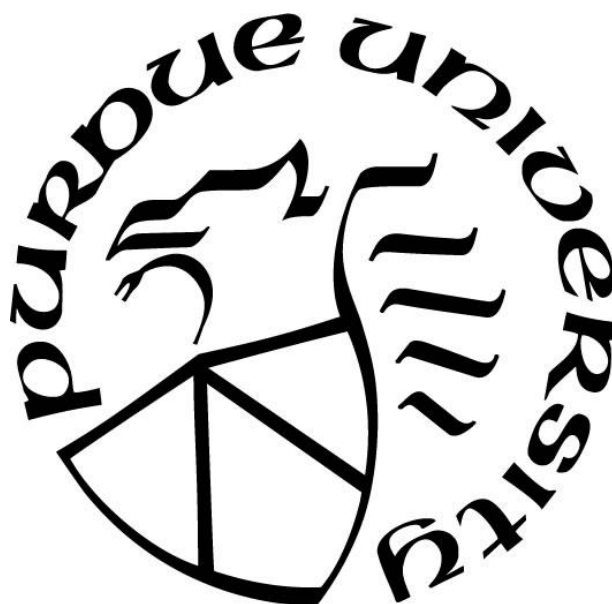
by

Yan-Shu Huang

A Thesis

Submitted to the Faculty of Purdue University

In Partial Fulfillment of the Requirements for the degree of

Master of Science in Chemical Engineering

Davidson School of Chemical Engineering

West Lafayette, Indiana

August 2020

THE PURDUE UNIVERSITY GRADUATE SCHOOL
STATEMENT OF COMMITTEE APPROVAL

Dr. Gintaras V. Reklaitis, Chair

Davidson School of Chemical Engineering

Dr. Zoltan K. Nagy, Chair

Davidson School of Chemical Engineering

Dr. Marcial Gonzalez

School of Mechanical Engineering

Dr. Sangtae Kim

Davidson School of Chemical Engineering

Dr. Stephen P. Beaudoin

Davidson School of Chemical Engineering

Approved by:

Dr. John A. Morgan

Dedicated to my parents for their constant support and love

ACKNOWLEDGMENTS

TABLE OF CONTENTS

LIST OF TABLES

LIST OF FIGURES

ABSTRACT

To continue the shift from batch operations to continuous operations for a wider range of products, advances in real-time process management (RTPM) are necessary. The key requirements for effective RTPM are to have reliable real-time data of the critical process parameters (CPP) and critical quality attributes (CQA) of the materials being processed, and to have robust control strategies for the rejection of disturbances and setpoint tracking.

Real-time measurements are necessary for capturing process dynamics and implement feedback control approaches. The mass flow rate is an additional important CPP in continuous manufacturing compared to batch processing. The mass flow rate can be used to control the composition and content uniformity of drug products as well as an indicator of whether the process is in a state of control. This is the rationale for investigating real-time measurement of mass flow of particulate streams. Process analytical technology (PAT) tools are required to measure particulate flows of downstream unit operations, while loss-in-weight (LIW) feeders only provide initial upstream flow rates. A novel capacitance-based sensor, the ECVT sensor, has been investigated in this study and demonstrates the ability to effectively measure powder mass flow rates in the downstream equipment.

Robust control strategies can be utilized to respond to variations and disturbances in input material properties and process parameters, so CQAs of materials/products can be maintained and the amount of off-spec production can be reduced. The hierarchical control system (Level 0 equipment built-in control, Level 1 PAT based PID control and Level 2 optimization-based model predictive control) was applied in the pilot plant at Purdue University and it was demonstrated that the use of active process control allows more robust continuous process operation under different risk scenarios compared to a more rigid open-loop process operation within predefined design space. With the aid of mass flow sensing, the control framework becomes more robust in mitigating the effects of upstream disturbances on product qualities. For example, excursions in the mass flow from an upstream unit operation, which could force a shutdown of the tablet press and/or produce off-spec tablets, can be prevented by proper control and monitoring of the powder flow rate entering the tablet press hopper.

In this study, the impact of mass flow sensing on the control performance of a direct compaction line is investigated by using flowsheet modeling implemented in MATLAB/Simulink to examine the control performance under different risk scenarios and effects of data sampling (sampling time, measurement precision). Followed by the simulation work, pilot plant studies are reported in which the mass flow sensor is integrated into the tableting line at the exit of the feeding-and-blending system and system performance data is collected to verify the effects of mass flow sensing on the performance of the overall plant-wide supervisory control.

1. INTRODUCTION

1.1   Background of Pharmaceutical Manufacturing

Pharmaceutical manufacturing is generally divided into upstream manufacturing and downstream manufacturing. Upstream manufacturing aims to produce drug substances, also known as active pharmaceutical ingredients (API), and typically includes one or more chemical synthesis steps followed by several separation unit operations such as crystallization, filtration, and drying. Downstream manufacturing serves to produce drug products by combing APIs and inactive ingredients, called excipients, to create a dosage form humans can take. The oral solid dosage, tablet and capsule, is the most common dosage form because it is convenient for people to take and relatively simple for manufacturers to make, store, and distribute. Depending on material properties, tablets can be produced via different processing routes, including wet granulation, dry granulation or direct compaction.

Drug product manufacturing plays a key role in the part of the healthcare sector that deals with medications. However, while pharmaceutical companies use cutting-edge science to discover new medicines, they have been manufacturing them using out-of-date techniques [2]. Conventional tablet manufacturing mostly relies on batch processes, in which materials are tested off-line after each batch unit operation. If the critical quality attributes (CQAs) of the samples meet the specifications approved by the Food and Drug Administration (FDA), the materials can be sent to the next processing step. However, if the specifications are not met, then the whole batch must be discarded given its potential negative impact on human health. These wasted batches constitute enormous loss of money for pharmaceutical companies. Moreover, inefficient manufacturing can lead to drug shortages for the whole society. Therefore, how to efficiently utilize materials like APIs and maintain CQAs at the same time becomes an important issue for manufacturing research.

Continuous manufacturing provides a more promising approach to efficiently utilize materials than batch manufacturing, especially with the application of advanced process design, monitoring and control methods [3, 4]. For example, when using on-line monitoring of quality only intermediate

materials with acceptable characteristics would be advanced to the next unit operation in a continuous process. If some intermediate materials didn't meet the FDA expectations, then the continuous process could discard only those unqualified parts of the material flow and adjust control variables to ensure CQAs of the continuing materials in the process line, rather than shutting down the entire production line. Moreover, scale-up is relatively easy for continuous manufacturing because by simply increasing process time more products can be produced, which means neither larger equipment and space nor different operation conditions taking into account scale-up are needed [5]. However, continuous manufacturing is a very new idea for the pharmaceutical industry and only six solid oral drugs produced via continuous tablet manufacturing have been approved by the FDA to date [6-8]. Obviously, continuous manufacturing still faces some challenges such as online property measurement, modeling of integrated processes and supervisory control [3]. This research will focus on how to monitor powder mass flow rate in real-time and utilize mass flow measurement to improve control performance of a continuous solid oral dosage process.

The mass flow rate is an important critical process parameter (CPP) which affects the concentration and the content uniformity of final products. Those attributes depend on the relative amounts of APIs and excipients which are combined into the powder blend. Although loss-in-weight (LIW) feeders can deliver granular materials at specified set points, the actual mass flow measurements are still required to mitigate flow disturbances by applying strategies such as ratio control [9]. Moreover, the mass flow rate is an indicator of whether the process is in a state of control and is not subject to material losses or materials accumulations. Besides, the exit flow rate from the blender is a disturbance variable for downstream unit operations. Process variation caused by mass flow variation can be mitigated if the mass flow is measured and controlled in real time. Therefore, this research is focused on how to utilize sensors to capture the real-time mass flow, which is a prerequisite for effective real-time process management.

1.2   Research Objectives

The first objective is to investigate the application and comparative effectiveness of an Electric Capacitance Volume Tomography (ECVT) sensor and an X-ray based sensor for real-time measurement of mass flow of powder/granular flows.

The second objective is to investigate the impact of mass flow sensing on the control performance of a direct compaction line by using flowsheet modeling implemented in MATLAB/Simulink. Further, pilot plant studies are reported in which the mass flow sensor is integrated into the tableting line at the exit of the feeding-and-blending system and system performance data is collected to verify the effect of mass flow sensing on the performance of the overall plant-wide supervisory control.

2. REAL-TIME MASS FLOW MONITORING

2.1 Introduction

Process analytical technology (PAT) tools are required to measure particulate flows of downstream unit operations, since loss-in-weight (LIW) feeders can only provide the initial upstream flow rates in continuous tablet manufacturing. Methodologies developed to measure mass flow rate can be divided into direct methods and inferential methods including measurement of instantaneous particle velocity and instantaneous volume fraction. Direct measurement methods only provide the mass flow rate, such as thermal methods depending on the proportional relationship between mass flow and the ratio of the heat input to the temperature change. Another example is the active charging and detecting method, where the mass flow rate is proportional to the electrical current. Inferential methods are used in this research because they can provide more information than direct methods. For example, the measured velocity can be used not only in the calculation of the mass flow rate but also in fault monitoring. The inferential method can be represented as Eq. 2.1 [10]:

$$M_s(t) = \rho_s A V_s(t) \beta_s(t) \qquad\qquad \text{Eq. 2.1}$$

where $V_s(t)$ is the velocity, $\beta_s(t)$ is the volume fraction and $M_s(t)$ is the mass flow rate of solids. True density of solids ρ_s can be assumed to be a constant and the cross-sectional area A of the pipe is known. Based on different physical principles, several PAT tools have been proposed to measure the particle velocity and the volume fraction. The X-ray based sensor and the ECVT sensor will be discussed in this research.

The X-ray sensor is based on attenuation of a monochromatic electromagnetic wave through a particulate medium coupled with cross-correlation velocimetry. The X-ray attenuation follows Beer-Lambert's law as given by Eq. 2.2 [11]:

$$\beta_s = \frac{-ln(I/I_0)}{L_c \mu} \qquad\qquad \text{Eq. 2.2}$$

where I_0 and I are the intensities of the incident and transmitted X-ray respectively, L_c is the length of the chord across the pipe section, and μ is linear attenuation coefficient of the solid material. Higher particle volume fraction (β_s) is reflected in the attenuated intensity (I) of the transmitted X-ray. When the X-ray based sensor, manufactured by Enurga Inc., (West Lafayette, IN) was used in measuring powder blends composed of different proportions of APAP, MCC, lactose, magnesium stearate and silicon dioxide, the research reported by Ganesh et al [12] indicated that the mass flow rate could be measured within an accuracy of 5% of the actual mass flow rate in the pilot plant at Purdue University. While the measurement accuracy was acceptable, the location of the X-ray sensor is limited because of the requirement for bulky and heavy lead shielding. This limitation has motivated the investigation of alternative technologies.

The ECVT sensor is based on the principle of parallel-plate capacitor as defined by Eq. 2.3 [13] where the dielectric permittivity of dilute solid-gas mixtures can be represented by Eq. 2.4 [14]:

$$C = \varepsilon \frac{A_p}{d} \qquad \text{Eq. 2.3}$$

$$\varepsilon = \beta_s \, \varepsilon_s + (1 - \beta_s) \, \varepsilon_{air} \qquad \text{Eq. 2.4}$$

where ε, ε_s and ε_{air} are the permittivity of mixture, solids and air respectively. C is capacitance, A_p is the area of the plate, d is the distance between two plates and β_s is the volume fraction of solids. A higher mass flow rate is reflected in higher permittivity and thus capacitance.

According to the literature [10], variations in particle size influence the operation of most sensors except those based on capacitance and radiometric principles. However, these sensors are very sensitive to moisture content. For instance, a variation of 1% moisture in coal has been reported to result in a 25-30% variation in the measured solid fraction obtained by utilizing capacitance-based sensors. This indicates that while particle size may not be an important factor, moisture can have an important negative effect on the accuracy of the measurement. Nonetheless, capacitance-based sensors are widely used in systems involving pneumatically conveyed particles [15-17], but are rarely used in the pharmaceutical industry. Guo et al [18] reported that the accuracy of mass flow measurement of pulverized coal conveyed pneumatically in downward flow orientation was

16

within 5% while Li et al [19] indicated the error of mass flow measurement of gravity-fed glass beads ranged between -3% to 8%. These reports suggest that the ECVT sensor should be able to perform to comparable error limits when used with pharmaceutical powder blends.

2.2 Materials and Methods

2.2.1 Materials

Acetaminophen Grade 0048 (APAP) was purchased from Mallinckrodt (Raleigh, NC). Avicel microcrystalline cellulose Grade PH-102 (MCC-102) and Grade PH-200 (MCC-200) were purchased from FMC BioPolymer (Philadelphia, PA). Lactose monohydrate Grade 310 was purchased from Kerry Inc. (Jackson, WI). Silicon dioxide was used as glidant. All powder blends were prepared by using a 5L Tote blender for 30 min.

2.2.2 ECVT Sensor Description

The Electrical Capacitance Volume Tomography (ECVT) sensor, offered by Tech4Imaging LLC, (Columbus, OH), is a non-invasive sensing technology with fast data acquisition. Figure 2.1a shows the structure of one example of the ECVT sensor. In the design used in these experiments, the sensor consists of 12 small plates, where 4 of those 12 plates are disconnected and each 2 small plates of the other 8 plates are combined into a large plate. The plate 1 and the plate 2 can be viewed as a top parallel-plate capacitor, while the plate 3 and the plate 4 can function as a bottom parallel-plate capacitor.
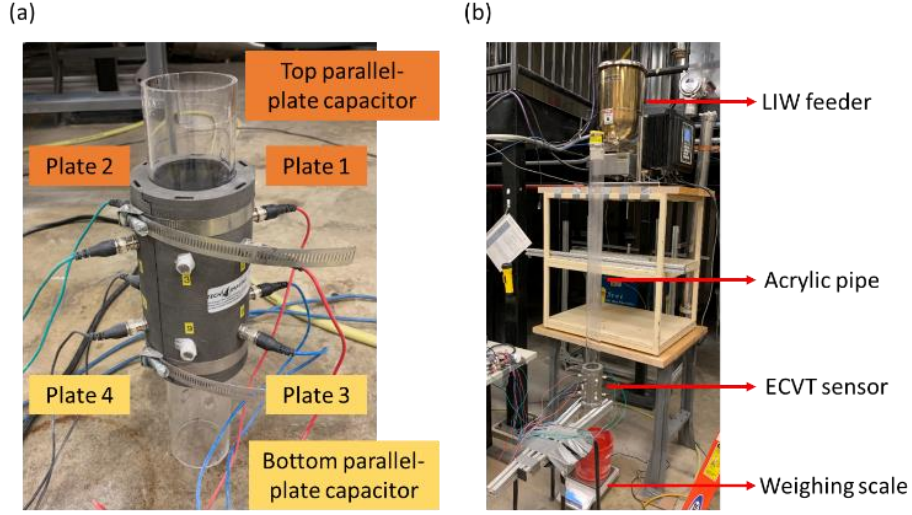
Figure 2.1 Sensor configuration: (a) ECVT sensor (b) stand-alone system

2.2.3 Experimental Setup

A stand-alone system consisting of a K-Tron KT20 loss-in-weight (LIW) feeder, the ECVT sensor and an independent Mettler-Toledo ME 4001E weighing scale for gravimetric measurement is shown in Figure 2.1b. The ECVT sensor does not provide the actual capacitance, as only normalized capacitance can be measured, following Eq. 2.5 where intensity (I) is an integer value between -65536 and 65535. During initial calibration of the ECVT sensor, the normalized capacitance of the empty pipe is 0 and that of the pipe filled with solid materials is 1. The AC excitation frequency is set to 62.5 kHz during initial calibration. When experiments are performed, the powders are loaded into the hopper of the LIW feeder, then fed into an ID 6.35 cm acrylic pipe that is surrounded by the ECVT sensor. At each measurement, one minute of no flowing material at the beginning and in the end are used to detect the extent of measurement drift and fouling.

$$C_{normalized} = \frac{I_{measured} - I_{empty}}{I_{full} - I_{empty}} = \frac{1}{k} \frac{C - C_{air}}{C_s - C_{air}} = \frac{1}{k} \beta_s \qquad \text{Eq. 2.5}$$

2.2.4 Data Analysis

The measurement of the velocity of solids is based on cross-correlation velocimetry, which transforms the time delay of signal between the top capacitor and the bottom capacitor into velocity as shown in Figure 2.2a. Due to mass balance, areas under the curves of mass flow rate versus time from the weighing scale and those from the ECVT sensor should be the same. However, given sensor baseline drift problems and fouling problems, this calibration method can cause underestimation of mass flow rates from the ECVT sensor. Therefore, in this study, the capacitance data are used to compute differences between the values when there is no flow of materials and the values recorded during flow of materials, shown as values C_1 or C_2 in Figure 2.2b. The average of C_1 and C_2 is used in sensor calibration similarly to determining a scaling factor, as shown in Eq. 2.5. The transient velocity is relatively stable, so the averaged velocity can be used in sensor calibration.
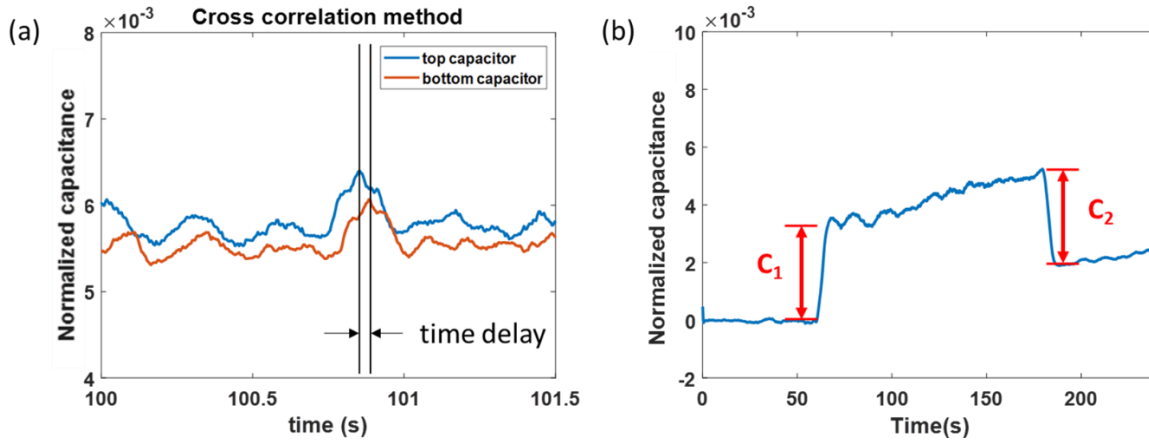
Figure 2.2 Illustration of how to analyze (a) velocity and (b) capacitance

19

2.3   Results and Discussions

2.3.1   Effects of L/D Ratio

The ECVT sensor must be located in an appropriate position in the pipe because the length (L) between the exit of the LIW feeder and the sensor affects the velocity measurement. As shown in Figure 2.3, when MCC-200 was fed into the pipe with inner diameter (D) 6.35 cm at flow rate 5 kg/hr, the velocity measurement from the sensor setup with length 104.8 cm (L/D = 16.5) was more stable than results from the same setup with length 33.5cm (L/D = 5.3). This is attributed to the fact that a low L/D ratios there is insufficient time for free-falling powders to achieve a stable terminal velocity in the downward direction [20].
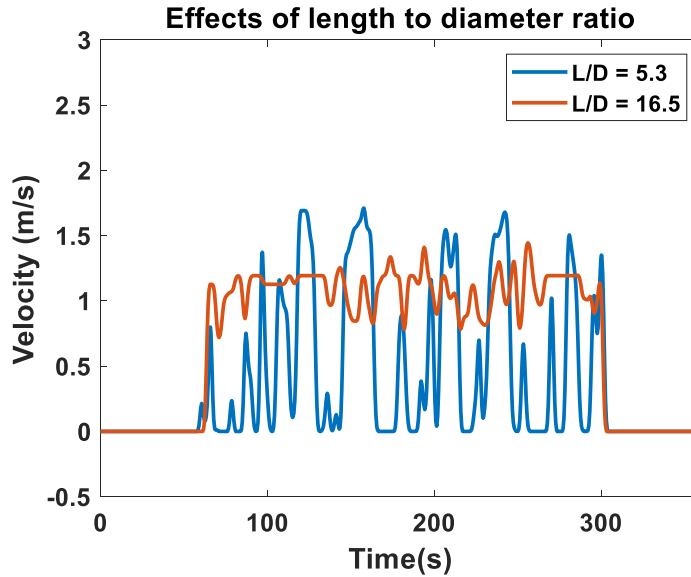
Figure 2.3 Effects of length to diameter ratio on the velocity measurement

2.3.2 Effects of Mass Flow Rates

The model material MCC-200 was fed at various flow set points from 2 kg/hr to 10 kg/hr. The capacitance increased with increased mass flow rates because the increased amount of MCC-200 powders increased permittivity of the gas-solid mixture within the sensing space as shown in Figure 2.4a. The velocity when the setpoint was between 6 kg/hr and 10 kg/hr was close to the same value of around 1.1 m/s as shown in Figure 2.4b. However, the velocity variation was too large to be viewed as a robust velocity when set points were too low, such as situations with set points below 4 kg/hr. The velocity sometimes could drop to zero, such as in the situation of the set point equal to 2 kg/hr, and that could be attributed to failure of cross-correlation velocimetry, which means signals from top and bottom capacitors were not similar enough so time delay found by the algorithm was 0 s, and thus the computed velocity approached infinity. Therefore, the algorithm was modified so that the infinity value was reset to zero to indicate a failure in velocity measurement using the velocity of 0.

(a) (b)
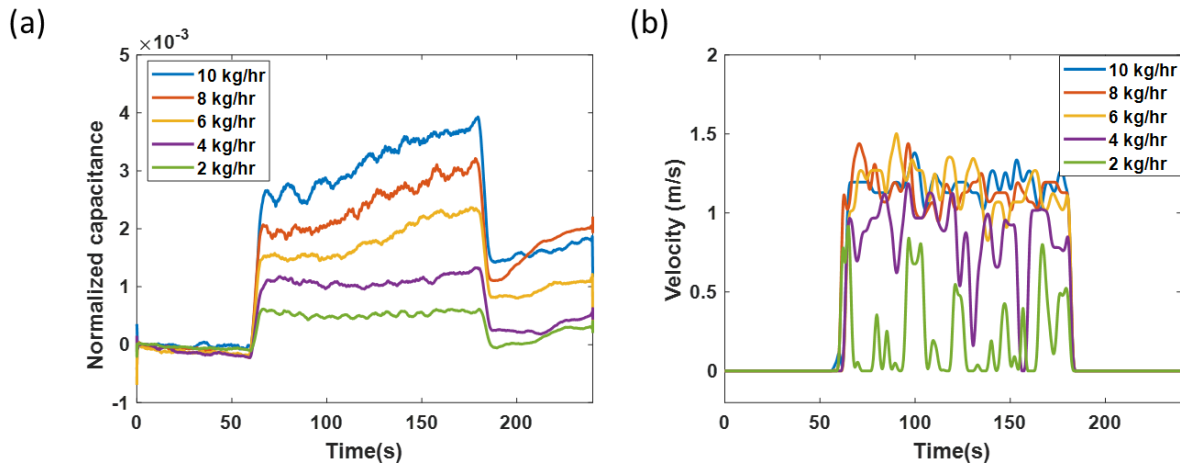
Figure 2.4 Time series data (a) normalized capacitance and (b) velocity at different set points

2.3.3 Effects of Powder Properties

To test the effects of powder bulk density, particle size, and API concentration, five kinds of powders given in Table 2.1. True density of the particle is its density excluding any pores and is the density of the solid material, which is assumed to be a constant. Bulk density of a powder is

the density when the powder is in a state of incipient fluidization, which means a loose or poured powder is used in bulk density measurement. The variation in bulk density is the largest among all kinds of density, because bulk density can be easily affected by slight shaking, humidity, pressure, or the height where the powder is delivered. That's the reason to investigate the effects of the bulk density. Tapped density of a powder is the bulk density of the powder after it has been subject to a prescribed style of tapping over a prescribed period of time. Tapped density can be used to calculate Hausner Ratio, which is defined as the ratio of the tapped density to the bulk density and is the most commonly used quantity to determine flowability in the pharmaceutical industry. Smaller Hausner ratio means better flowability of the powder, so MCC 200 with the best flowability is suitably used as a model material to calibrate the mass flow sensor.

Five kinds of powders were measured at three different mass flow rates, and their values averaged over two minutes are shown in Figure 2.5 including the normalized capacitance (Figure 2.5a), the velocity (Figure 2.5b) and predicted mass flow rates from the ECVT sensor (Figure 2.5c).

Table 2.1 Powder properties

	True density (g/mL)	Bulk density (g/mL)	Tapped density (g/mL)	Hausner ratio	d_{50} (μm)
Lactose	1.590	0.596	0.817	1.37	92
MCC-102	1.471	0.356	0.422	1.19	100
MCC-200	1.456	0.375	0.425	1.13	200
MCC-200(90%) +APAP(10%)	1.449	0.344	0.410	1.19	N/A
MCC-200(80%) +APAP(20%)	1.427	0.356	0.426	1.20	N/A

First, effects of particle size could be observed from the results with MCC-200 (median size ~ 200 μm) and those of MCC-102 (median size ~ 100 μm). At the same mass flow rates, the velocity of MCC-102 (0.9 m/s) is slightly smaller than that of MCC-200 (1.1 m/s) due to size effects [21]. The volume fraction is inversely proportional to the velocity, which is verified by the fact that capacitance of MCC-102 was larger than that of MCC-200. The higher error (≤12.7%) of mass

flow rate of MCC-102 than of MCC-200 ($\leq 7.7\%$) may be attributed to fouling caused by poor flowability of the material with smaller particle size.

Secondly, effects of bulk density could be observed from the results of MCC-102 (0.356 g/cm^3) and those of lactose (0.596 g/cm^3). At the same screw speed, lactose was discharged at higher mass flow rate and higher velocity than MCC-102. The highest velocity of lactose among all materials results in the lowest capacitance. The errors of mass flow rate are similar in both materials, indicating that the accuracy of mass flow rate should not have a strong dependence on bulk density.

Thirdly, effects of the composition of API could be observed from the results of MCC-200, Blend 10% (10%APAP + 90%MCC-200) and Blend 20% (20% APAP + 80%MCC-200). The velocity of these three materials is similar at the same mass flow rates. However, the error of the capacitance and mass flow rates of Blend 10% and Blend 20% are higher than those of MCC-200, which may be attributed to content uniformity of APAP in blends and different permittivity of MCC-200 and APAP.

(a)

MCC-102
Lactose

MCC-200
MCC-102

MCC-200
Blend 10%
Blend 20%

(b)

MCC-200
Lactose

MCC-200
MCC-102

MCC-200
Blend 10%
Blend 20%

(c)

- MCC-200
- Blend 10%
- Blend 20%
- MCC-102
- Lactose

Materials	Scaling factor k	Error (%)
MCC 200	0.206	0.4~7.7
Blend 10% (10%APAP + 90% MCC200)	0.192	2.3~15.9
Blend 20% (20%APAP + 80% MCC200)	0.215	1.5~14.1
MCC 102	0.183	0.3~12.7
Lactose	0.178	1.2~12.2
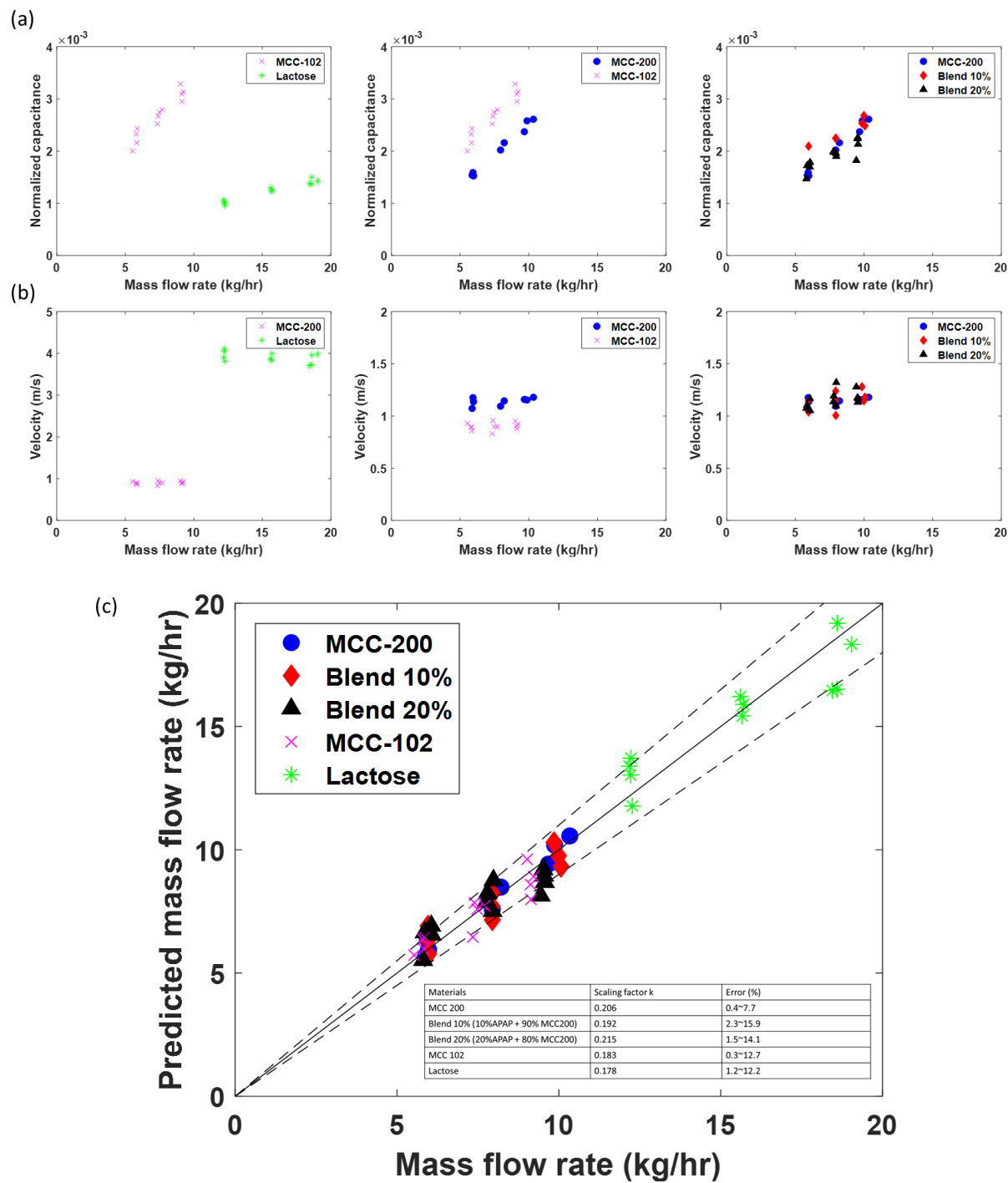
Figure 2.5 Effects of powder properties including bulk density, particle size and concentration of API on (a) velocity, (b) normalized capacitance and (c) predicted mass flow rates

24

2.3.4 Approaches to Improve Measurement Accuracy

Compared to the measurement errors of 5% obtained with the X-ray sensor, the measurement accuracy of the ECVT needs improvement for further implementation in the manufacturing line. The challenges to enhance measurement accuracy are to mitigate the effects of sensor baseline drift and fouling on the pipe. Therefore, several approaches have been investigated and results are discussed in this chapter.

Sensor baseline drift can in part be attributed to temperature variations in the printed circuit board (PCB) of the data acquisition system [10]. Figure 2.6 shows that the capacitance (blue dashed line) of an empty pipe and the circuit board temperature (red line) are positively correlated. The increased value of 0.0011 for capacitance variation caused by increased 0.5°C temperature variation appears to be not serious, but it does result in a huge negative impact on mass flow accuracy in the dilute free-falling solid-gas system when the solid fraction is less than 0.1% and the capacitance is less than 0.01. Accordingly, a temperature compensation technique can be used in which the relationship between the capacitance and the temperature is assumed to be linear providing that the temperature is only subject to small variations. When the linear temperature compensation technique is applied, the sensor drift is reduced from 0.0011 to 0.0002 considering the difference between the incipient capacitance and the capacitance at $t = 1200$ sec.
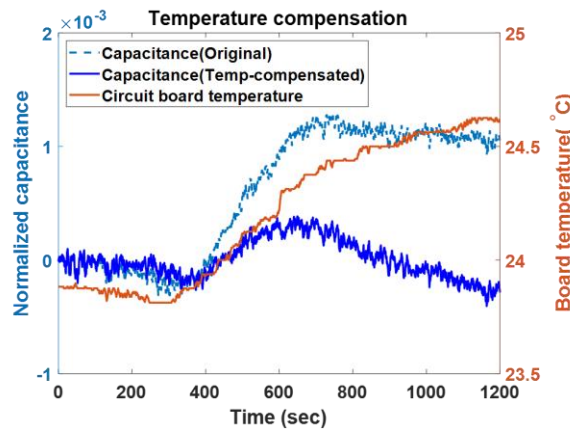
Figure 2.6 Sensor baseline drift caused by temperature variations in the PCB

Another approach to alleviate the effect of sensor drift is to reduce the diameter of the ECVT sensor. Although reduced diameter does not directly lessen the drift extent, when the inner diameter of the sensor is reduced from 2.5 inches to 1 inch, the capacitance signal of the powder fraction is amplified, which consequently mitigates the impact of sensor drift. However, the reduced diameter can worsen the effects of fouling on the pipe because a layer of powder adhesion with the same thickness accounts for a larger proportion in the 1 inch pipe than in the 2.5 inch pipe.

Figure 2.7 shows the situation when fouling takes place and the situation when fouling is mitigated. Powders adhering to the pipe wall can result in overestimation of measured powder flow rates, and the time-variant extent of fouling produces gross error and large variations in sensor measurement. Therefore, a vibration device was fixed on the pipe to help remove the powders adhering to the pipe wall. Figure 2.8a indicates that accumulated fouling makes mass flow measurement from the ECVT sensor increase gradually, resulting in a large deviation compared to the actual mass flow rate from the weighing scale. With the aid of the vibration device, fouling is mitigated and the measurement error is decreased as shown in Figure 2.8b. It should be noted that the reading of the ECVT sensor is not negatively affected by vibration, whereas such vibrations can strongly affect the mass flow reading when using load cell based techniques, which are used in LIW feeders.
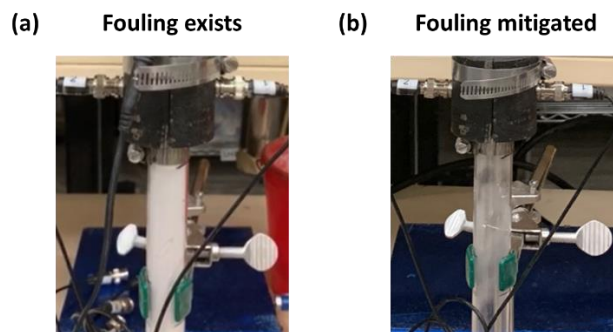
Figure 2.7 Illustration of fouling in the pipe
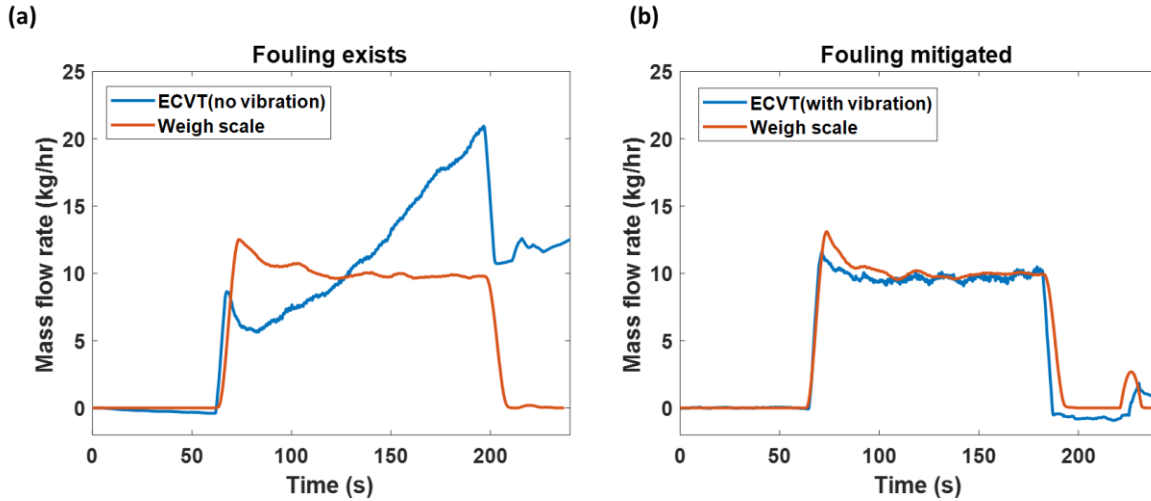
Figure 2.8 Effects of vibration on fouling

Given that powders sometimes could be too cohesive to be shaken off by a vibration device, the effects of pipe materials on powder adhesion was also considered. Adhesivity and electrostatic chargeability of the powders are two main reasons for fouling [22]. Accordingly, the effects of choice of three pipe materials, polytetrafluoroethylene (PTFE), polyvinyl chloride (PVC) and polycarbonate, were investigated. The friction coefficients and work functions [23] for these materials are listed in Table 2.2. Pipes with lower friction coefficient can reduce the amount of powder that adheres to the pipe wall. In these experiments MCC-200 is blended with 0.2 wt% SiO_2 to increase the powder flowability. Providing that the work function of MCC is 5.11 eV [23], PVC can reduce the tribocharging effect the most. It can be expected that materials with higher work function will tend to charge with positive polarity and thus that larger difference in work function between two materials will result in more accumulated static charges.

Mass flow rates from the weighing scale in the top part of Figure 2.9 suggest that powder flow rates are steady after t = 100 sec at five different flow rates. In other words, mass flow rates from the ECVT after t = 100 sec as shown in the bottom part of Figure 2.9 theoretically should be as steady as possible. In addition, the difference between the capacitance of the first minute and the capacitance of the last minute is caused by the change of the amount of powder fouling. Based on these criteria, PTFE is the preferred candidate to reduce the effects of fouling. These results also indicate that fouling of MCC-200 is more subject to the friction coefficient than to the work

27

function considering that PVC (5.13 eV) is closest to the work function of MCC (5.11 eV). The polycarbonate is the worst choice for measuring mass flow rates of MCC-200 because of the highest friction coefficient. One additional point worth noting from Figure 2.9 is that the ECVT measurement can reflect the mass flow variation very well even when powder flow rates are low (2 kg/hr, green line). It is evident from these experiments that several mitigation strategies must be employed to minimize the effects of sensor baseline drift and fouling and thus to enhance measurement accuracy. The average errors of the predicted mass flow are listed in Table 2.3, which also includes the mass flow error by using 2.5 inch pipe for comparison. To calculate average errors of ECVT sensors, the average mass flow rates over 1 minute (from t = 100 sec to 160 sec) from both the weighing scale and the ECVT are used, which is (Rate $_{ECVT}$ – Rate $_{Weigh}$) / Rate $_{Weigh.}$ The error range provided in Table 2.3 includes all the errors within the listed flow range. For 1 inch sensor with different pipe materials, there is one measurement for five setpoints (2, 4, 6, 8, 10 kg/hr). For 2.5 inch sensor used for different powders, there are three measurements for three setpoints. The results indicate the best measurement accuracy is achieved by using 1 inch PTFE pipe, supported by the value of the smallest error (-1.8 ~ 3.3%).

Table 2.2 Pipe properties

	PTFE	PVC	Polycarbonate
Friction coefficient	0.04	0.20	0.31
Work function (eV)	5.75	5.13	4.68
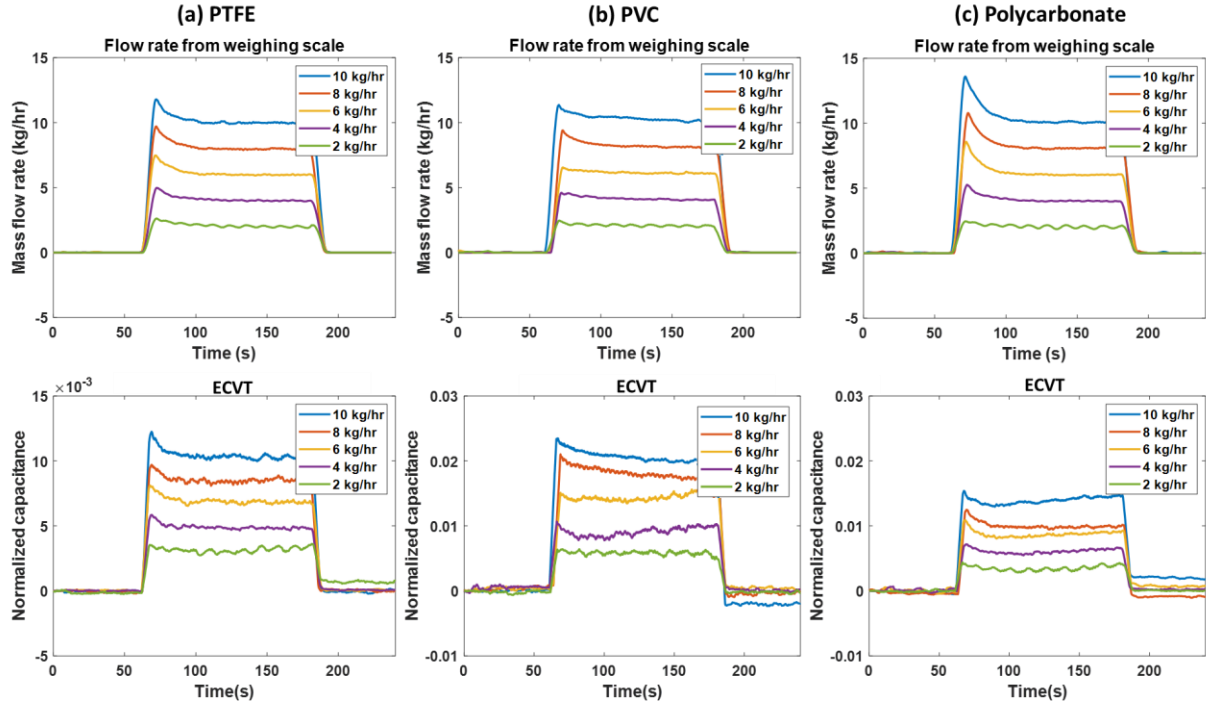
Figure 2.9 Effects of pipe materials including (a) PTFE, (b) PVC, and (c) polycarbonate

2.4　Conclusions

The novel capacitance-based ECVT sensor shows the ability to distinguish different mass flow rates from 0 to 20 kg/hr. To capture stable velocity, the L/D ratio of the section of flow upstream of the location at which the flow sensor is positioned should be large enough for the free-flowing powder to reach its terminal velocity. Moreover, cross-correlation velocimetry is more accurate at relatively high flow rates (e.g. MCC-200 at 10 kg/hr) than at low flowrates (e.g. MCC-200 at 2 kg/hr). In a dilute free-falling solid-gas system, the capacitance plays a more important role in reflecting the real mass flow rates than the velocity which depends on powder properties rather than mass flow rates. The effects of powder properties including the bulk density, the particle size, and the API composition are investigated in this study. The experimental results allow three conclusions to be drawn: (1) higher bulk density results in lower capacitance and higher velocity,

29

(2) larger particle size results in lower capacitance and higher velocity, and (3) API compositions less than 20% do not affect either capacitance and velocity to any significant extent.

The two main root causes of the mass flow measurement error are sensor baseline drift and sensor fouling. These two factors can worsen the accuracy of ECVT measurement especially in the case of dilute solid-gas systems. Temperature compensation technique can be used to mitigate sensor drift caused by temperature variations in the printed circuit board of the data acquisition system. In addition, when the diameter of the pipe passing through the ECVT sensor is reduced from 2.5 inches to 1 inch, the capacitance signal of powder fraction is amplified, which further mitigates the impact of sensor drift. To deal with the fouling issue, a small amount of glidant silicon dioxide can be added to the powder blend, thus improving the flowability of powders and reducing the pipe wall friction. Considering the work function and the friction coefficient of pipe materials, PTFE pipe can be used to reduce fouling the most. To obtain satisfactory real-time mass flow measurement for applications such as process control, approaches such as those investigated in this work are required to mitigate sensor drift and fouling.

As shown in this work by appropriate choices of upstream pipe length, pipe diameter relative to mass flow rate, pipe material of construction, use of a vibration device and inclusion of a small amount of glidant, the presentation of the powder flow to the sensor can be stabilized and fouling significantly reduced. The sensor signal itself also must also be corrected for the temperature of its printed circuit. With these engineering solutions applied, the experimental results summarized in Table 2.3 show that sensor measurement error can be reduced to between -1.8% and 3.3% depending on the absolute value of the mass flow.

Table 2.3 Average errors of the predicted mass flow rates from the ECVT sensor

Pipe	Powder material	Flow range (kg/hr)	Average error (%)
1 inch PTFE	MCC200 + 0.2%SiO2	2 ~ 10	-1.8 ~ 3.3
1 inch PVC	MCC200 + 0.2%SiO2	2 ~ 10	-8.5 ~ 5.6
1 inch Polycarbonate	MCC200 + 0.2%SiO2	2 ~ 10	-10.0 ~ 3.9
2.5 inch Acrylic	MCC200	6 ~ 10	-4.5 ~ 7.7
	Blend 10%	6 ~ 10	-7.4 ~ 15.9
	Blend 20%	6 ~ 10	-13.8 ~ 14.1
	MCC102	6 ~ 10	-12.6 ~ 10.0
	Lactose	12 ~ 20	-11.2 ~ 12.2

3. APPLICATIONS OF MASS FLOW MEASUREMENT TO PROCESS CONTROL

3.1 Introduction

The approach to quality control can be changed significantly with the shift from batch manufacturing to continuous manufacturing. The traditional method, known as Quality-by-Testing (QbT), is to test intermediate materials and final products at the end of each batch unit operation [24]. Open-loop process operation within the predefined design space or the documented recipe should be followed to meet a tight release specification regulated by the FDA. For example, as the specific amount of API and excipients are mixed in a fixed time period in a batch blender, thief sampling at discrete time points is required to check the blend homogeneity [25]. The control strategy in batch processes relies on using a simple programmable logic control (PLC) panel in each equipment. Although there are reports of advanced control strategies used in batch manufacturing, for example, the use of nonlinear model predictive control (NMPC) in a batch crystallizer [26], the advanced control strategy is still limited to individual unit operations rather than the entire process line.

Recognizing that testing and simple PLC control cannot provide real-time remedial control actions, the FDA has advanced the concept of Quality-by-Design (QbD) and issued some guidance documents [27-30]. The key message of QbD is that the quality must be designed into the product to reduce quality crisis drug manufacture [31]. With the aid of PAT tools and process understanding, the systematic design of operating space can be used to integrate each unit operation and to enable continuous manufacturing. Simultaneously, closed-loop plant-wide control is required in an integrated line to exercise corrective actions when the results of real-time release testing indicate that product is out of specification. To move from open-loop operation in one equipment to closed-loop operation in a plant-wide system, indispensable steps include control system design, control hardware/software and sensor integration, and control system implementation [32]. More recently, the QbD concept has been extended to a new concept called Quality-by-Control (QbC), which serves to address operating problems resulting from process disturbances and uncertainties as well as to provide more robustness and efficiency compared to

QbD approaches [1]. The benefits of the QbC approach are in part attributable to the active control approaches applied, with the proof-of-concept studies include the continuous tableting process [1, 33], the dry granulation process [34, 35], the drop-on-demand additive manufacturing process [36, 37] and the continuous crystallization process [38, 39].

A number of common control strategies (e.g. PID, MPC, feedforward, feedback) have been investigated in continuous pharmaceutical manufacturing under the guidance of QbD and QbC, but the most suitable and robust control system design has not yet been thoroughly developed [3, 40, 41]. The continuous direct compaction process has seen the most case studies investigating the process control strategies. For instance, Singh et al indicated that a hybrid MPC-PID control strategy with the API composition measurement using NIR was able to control the API composition better than a base level PID control scheme [40]. Another example is a study in which the coupled feedforward/feedback control with the bulk density measurement by using NIR was shown to reduce variations in CQAs [42]. However, the application of a mass flow sensor for the plant-wide control system has not been reported due to limited PAT tools for mass flow monitoring. Given that the powder flow rate is a disturbance variable to the downstream unit operations (the blender and the tablet press) and can impact CQAs (e.g. API composition) and CPPs (e.g. hopper level) in continuous manufacturing, this study will focus on the application of mass flow measurement to enhance control robustness and performance in a direct compression process.

3.2   Process Description

A direct compression line consists of three types of unit operations : Loss-in-weight (LIW) feeders, a blender, and a tablet press as shown in Figure 3.1. Loss-in-weight feeders are devices in which powder is fed from a hopper into a barrel which contains a rotating screw element. The entire device is set on a load cell and the difference in load cell weight measurements over a short time interval is used to compute an estimate of the mass flow. The computed flow is compared to the set point value and the screw rpm adjusted using a suitable control strategy to minimize the difference. The API and excipients are dispensed at target flow rates from respective LIW feeders and fed into a blender. In the blender, a rotating paddle causes mixing of the powders to a degree

33

sufficient to meet composition variation targets. Upon exiting the blender, the blend is transferred by gravity flow to the tablet press. At the exit of the blender, the mass flow sensor (e.g. ECVT) and the API concentration sensor (e.g. NIR) are used to measure the flow and composition values in real time as shown in Figure 3.1 (blue line). The blend flows into the hopper associated with the tablet press, then into the feed frame which next pushes the blend into the individual dies of the tablet press. Once the blend fills the die, the upper and lower punches compress the blend to form tablets, which are finally ejected by lower punches and collected at the end of the process as shown in Figure 3.1 (red dash line).
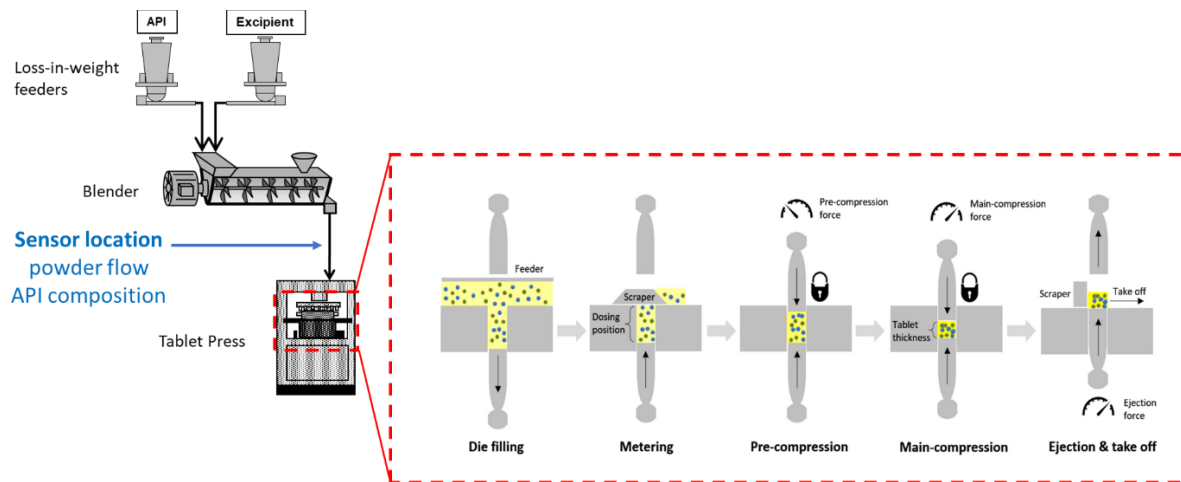
Figure 3.1 Process description of a direct compaction line

3.2.1 Models for Unit Operations

LIW Feeders

There are two available models for LIW feeders. One is a first order plus time delay (FOPTD) model as below.

$$\tau \frac{dy(t)}{dt} = -y(t) + K u(t - \theta) \qquad \text{Eq. 3.1}$$

$$\frac{Y(s)}{U(s)} = \frac{K}{\tau s + 1} e^{-\theta s} \qquad \text{Eq. 3.2}$$

where τ is the time constant, K is the process gain and θ is the time delay. Eq 3.2 is the Laplace transform of Eq 3.2. The other model is the feed factor model [43], which is better to capture process dynamics considering that the screw rotation speed has to vary according to the varying powder weight in the hopper and the effective bulk density of powders. The feed factor model is represented as below.

$$F = ff(t)\, \omega_{screw}(t) \qquad \text{Eq. 3.3}$$

$$ff(t) = \rho_{eff}(t) V_{screwpitch} \qquad \text{Eq. 3.4}$$

$$\rho_{eff}(t) = \rho_{sat} + e^{\frac{-\sigma_v(t)}{\beta}}(\rho_{ini} - \rho_{sat}) \qquad \text{Eq. 3.5}$$

$$\sigma_v(t) = \frac{m(t)g}{A_{feeder}} + \cos(2\pi\omega_{impeller}t)\frac{M_{blade}R_{blade}\omega_{impeller}^2}{A_{screwport}} \qquad \text{Eq. 3.6}$$

$$\omega_{impeller}(t) = \alpha\omega_{screw}(t) \qquad \text{Eq. 3.7}$$

$$\frac{dm(t)}{dt} = -F \qquad \text{Eq. 3.8}$$

where F is flowrate at the outlet of the feeder, ω_{screw} and $\omega_{impeller}$ are the feeder screw speed and impeller speed respectively, ff(t) is feed factor, $\rho_{effective}$ is the effective density, $V_{screwpitch}$ is the volume of the screw pitch, ρ_{sat} is the saturated density, ρ_{ini} is the initial density, σ_V is the vertical stress, β is the density constant, M_{blade} and R_{blade} are the mass and radius of the impeller blade, A_{feeder} and $A_{screwport}$ are the area of the feeder and the area of the port where screws enter the bowl, g is the gravity constant, m(t) is the powder weight in the feeder hopper and α is the impeller ratio between the impeller speed and the screw speed.

Blender

The blender is described by the two-dimensional (2D) compartment model [44, 45] which includes the axial and the radial direction. Each compartment is equally sized and assumed to be well mixed. The powder holdups of both the API and the excipient in each compartment is shown as below.

$$\frac{dm_{i,j}}{dt} = F_f\left(m_{i-1,j} - m_{i,j}\right) + F_b\left(m_{i+1,j} - m_{i,j}\right) + F_r\left(m_{i,j-1} - 2m_{i,j} + m_{i,j+1}\right) \qquad \text{Eq. 3.9}$$

$$F_f = a\omega_{blender} + b \qquad \text{Eq. 3.10}$$

$$F_b = c\omega_{blender} + d \qquad \text{Eq. 3.11}$$

$$F_r = e\omega_{blender} \qquad \text{Eq. 3.12}$$

where $m_{i,j}$ is the mass hold up in the compartment, i and j are the indices of the compartment in the axial and radial directions respectively. F_f, F_b and F_r are the forward, backward, and radial fluxes respectively, $\omega_{blender}$ is the blender rotation speed, and a,b,c,d and e are flux parameters. The blend flow at the exit of the blender is mainly determined by the powder holdups of the last compartments in the axial direction and the equations are represented as below.

$$F_{blender} = \sum_{j=1}^{n_r} F_{f,API}\, m_{API,i=n_a,j} + \sum_{j=1}^{n_r} F_{f,Exc}\, m_{Exc,i=n_a,j} \qquad \text{Eq. 3.13}$$

$$C_{API} = \frac{\sum_{j=1}^{n_r} F_{f,API}\, m_{API,i=n_a,j}}{F_{blender}} \qquad \text{Eq. 3.14}$$

$$RSD_{API} = \frac{\sqrt{\frac{1}{n_r-1}\sum_{j=1}^{n_r}\left(\frac{F_{f,API}\, m_{API,i=n_a,j}}{F_{f,API}\, m_{API,i=n_a,j}+F_{f,Exc}\, m_{Exc,i=n_a,j}} - C_{API}\right)^2}}{C_{API}} \qquad \text{Eq. 3.15}$$

where $F_{blender}$ is the powder flow rate at the exit of the blender, n_r and n_a are the number of the compartments in the radial and the axial direction respectively. C_{API} is the mean API composition of the blend. RSD_{API} is the relative standard deviation of the API used to quantify blend homogeneity.

Tablet Press

Tablet weight is determined by the amount of powders filling the die, and the variations of tablet weight may result from variations in the powder bulk density and die filling time as shown below.

$$W = \frac{\pi D^2 H_{fill}}{4} \rho_{bulk}(1 - c\omega_T) \qquad \text{Eq. 3.16}$$

$$F_{tablet} = W\omega_T N_{station} \qquad \text{Eq. 3.17}$$

$$\frac{dH_{hopper}}{dt} = \frac{F_{blender} - F_{tablet}}{\rho_{bulk} A_{hopper}}$$

Eq. 3.18

where W is the tablet weight, D is the diameter of the die, H_{fill} is the filling depth (or called dosing position), ρ_{bulk} is the powder bulk density, c is an efficiency parameter of powder flowing into the dies from the feed frame, and ω_T is the turret speed. F_{tablet} is the production rate of tablets and $N_{station}$ is the number of stations. The hopper level of the tablet press is determined by the inlet mass flow rate and the outlet mass flow rate, which are the flow rate at the exit of the blender and the production rate of tablets respectively.

The Kawakita model [46] is employed to describe the relationship between the main compression force and the relative density as follows:

$$CF = \frac{\pi D^2/4}{ab} \frac{1}{\left[\frac{1}{1-\rho_{cr}/\rho_r} - \frac{1}{a}\right]}$$

Eq. 3.19

$$\rho_r = \frac{W}{\frac{\pi D^2 H_{main}}{4} \rho_{true}}$$

Eq. 3.20

where CF is the main compression force, the parameter a is the maximum degree of compression, and the parameter b is the reciprocal of the pressure applied to the maximum degree of compression. ρ_r is the tablet relative density, which is the ratio of the tablet bulk density to the powder true density. ρ_{cr} is the critical relative density. H_{main} is the main compression thickness. For the powder blend, both the powder bulk density (ρ_{bulk}) and the powder true density (ρ_{ture}) are represented by the linear equations below.

$$\rho_{bulk}(t) = C_{API}\rho_{bulk,API}(t - \theta) + (1 - C_{API})\rho_{bulk,Exc}(t - \theta)$$

Eq. 3.21

$$\rho_{true}(t) = C_{API}\rho_{true,API}(t - \theta) + (1 - C_{API})\rho_{true,Exc}(t - \theta)$$

Eq. 3.22

where θ is time delay, which is assumed to be powder weight in the hopper divided by the tablet production rate. The detailed representation of flow sheet model is shown in Figure 3.2.
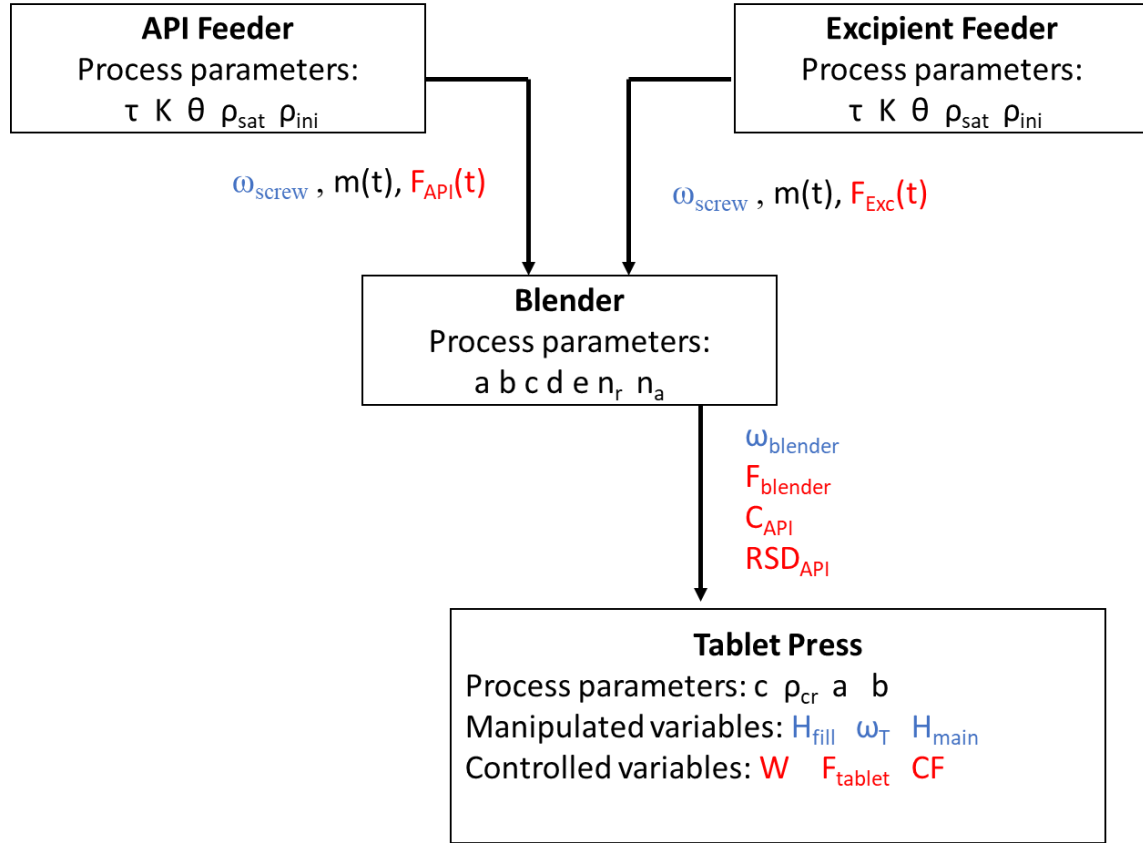
Figure 3.2 Detailed representation of flowsheet model for a direct compaction line

3.2.2 Hierarchical Three-Level Control Structures

According to the ISA-95 Enterprise-Control-System Integration Standard, the hierarchical three-level control structure is emphasized in the modern control system implementation with the levels classified according to their control objectives and can be represented by Figure 3.3(cited from [1]). The level 0 control technique is equipment based control, in which the control objectives are focused on the operation of the equipment itself. Simple PID control is generally implemented via a programmable logic control (PLC) panel in the equipment provided by the equipment vendor, and thus the CPPs can be directly manipulated and maintained within nominal operating conditions. For instance, the PLC in LIW feeders can deliver powder flow at the set point by adjusting the screw rotation speed, and the PLC in the blender can make the paddle rotate at a certain speed by adjusting the motor current.

The level 1 control is PAT based property feedback control, specifically, the measurements from PAT tools are used to control CQAs via suitable control logic. All the sensor data and the equipment data are collected in the Supervisory Control And Data Acquisition (SCADA) platform via OPC servers, and thus cascaded Single-Input Single Output (SISO) loops with PID controllers in the distributed control system (DCS) can be based on those measurements to supervise the level 0 PLC controllers. For example, the API composition at the exit of the blender can be adjusted by means of the control commands that the DCS sends to the PLC of the API feeder or the excipient feeder.

The level 2 control is model-based and optimization-based control of the entire production line. Mathematical models enable the DCS to validate the process measurements, to detect exceptional events and to predict the effects of variations in the CPPs on the CQAs. When the multivariable process is complex, the decoupled SISO control loops in level 1 could fail due to the strong interaction of process variables. Therefore, the advanced control strategy like model predictive control (MPC), which can deliver Multiple-Input Multiple-Output (MIMO) functionality, is needed to enhance process stability for plant-wide process control purposes.
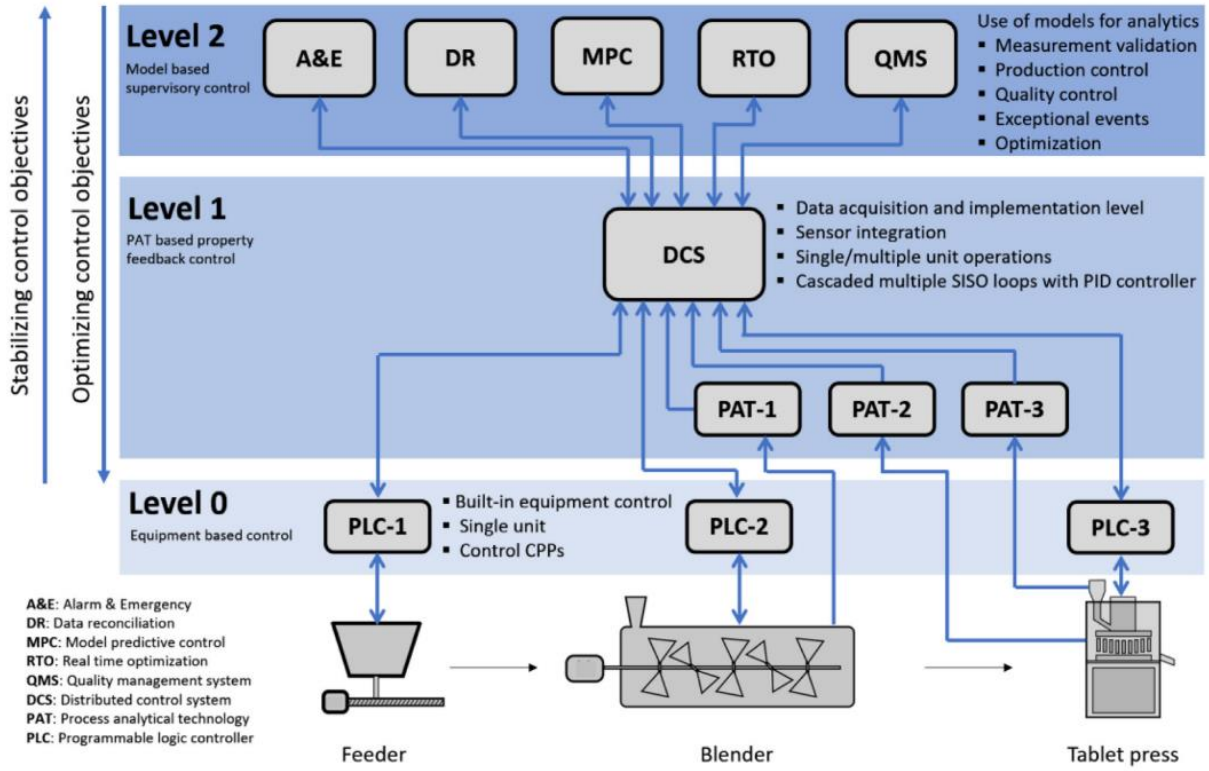
Figure 3.3 The hierarchical process control structure for a continuous direct compaction line [1]

MPC is based on iterative finite-horizon optimization of the process model. The objective function can be expressed as Eq. 3.23, in which the first term represents the weighted sum of squared errors of controlled variables (y) and the second term represents the weighted sum of controller adjustments (Δu).

$$\min_{\Delta u_j} J = \sum_{i=1}^{N_p} \sum_{j=1}^{n_y} W_j^y [y_j^{sp}(k+i) - y_j(k+i)]^2 + \sum_{i=1}^{N_c} \sum_{j=1}^{n_u} W_j^{\Delta u}[\Delta u_j(k+i-1)]^2 \quad \text{Eq. 3.23}$$

where k is the current sampling interval, (k+i) is the future sampling interval, N_p is the prediction horizon, N_c is the control horizon, n_y is the number of controlled variables, n_u is the number of manipulated variables, W_j^y is the weight for output y_j, $W_j^{\Delta u}$ is the rate weight, and y_j^{sp} is the set point of the controlled variable. The objective of MPC is demonstrated more clearly in Figure 3.4, which is to find the optimal first move for each manipulated variable during each iteration.
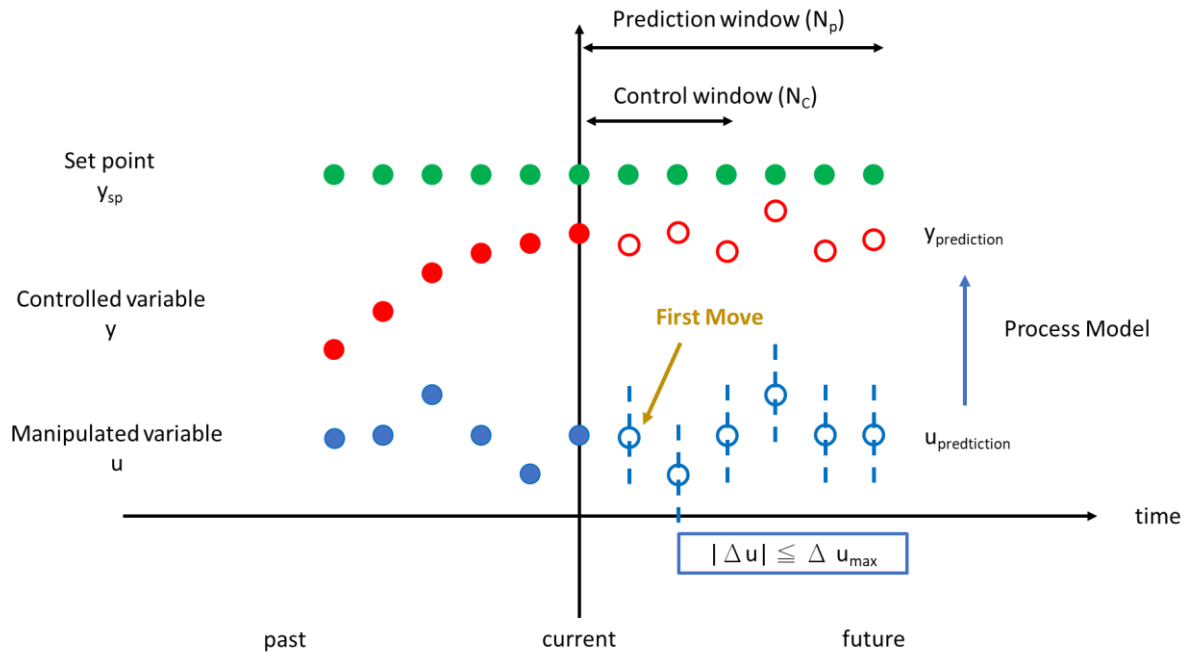
Figure 3.4 Illustration of model predictive control

3.3   Dynamic Flowsheet Modeling

Dynamic flowsheet models can serve as a digital surrogate for a real manufacturing process, so that evaluation of control strategies and the risk analysis can be done before the actual implementation of the physical process. The flowsheet model of the direct compaction process in MATLAB Simulink is shown in Figure 3.5, where blue lines represent the direction of materials flow and red lines represent the direction of measurement flow and control commands. The dynamic model equations in section 3.2 are written in MATLAB S-function files and thus can be executed in the Simulink environment.
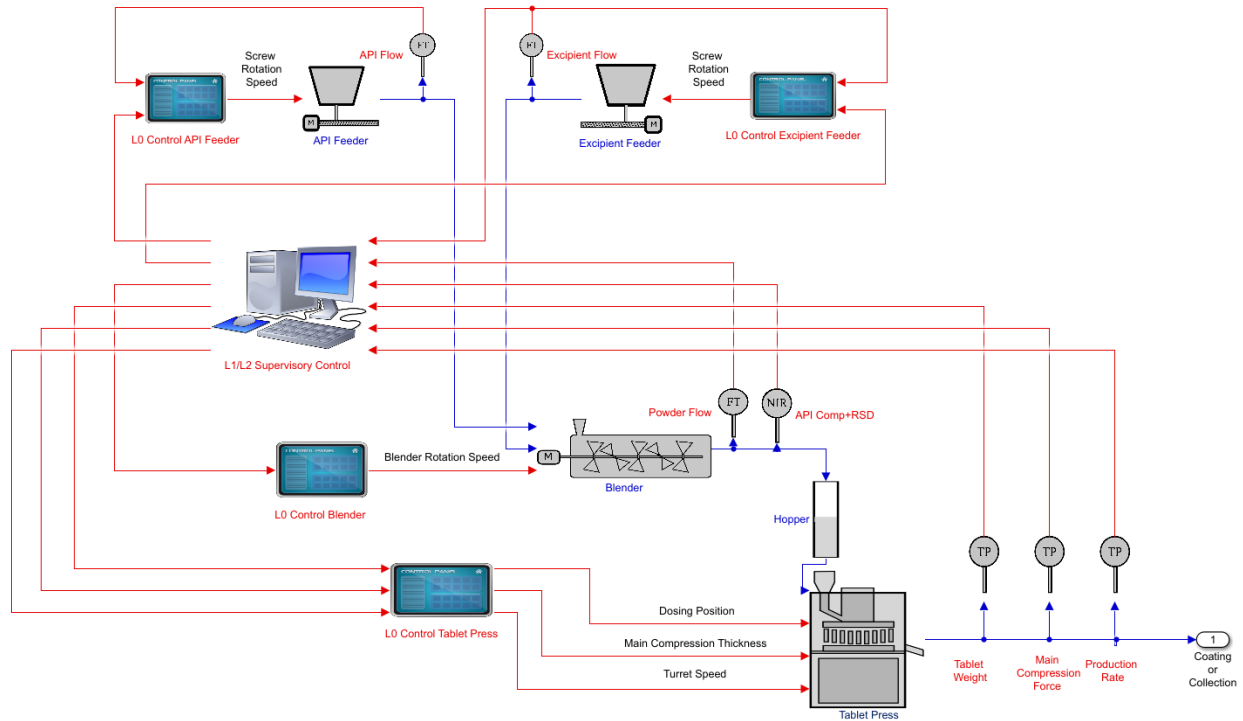
Figure 3.5 MATLAB Simulink flowsheet model of a direct compaction process

The hierarchical control structure is implemented in the DCS, namely 'L1/L2 Supervisory Control' subsystem in Figure 3.5, where all the process measurements are acquired. The detail of the 'L1/L2 Supervisory Control' is shown in Figure 3.6. The subscript m means measurement and the subscript sp means the setpoint. In this study, the 6 inputs by 6 outputs control structure is investigated with the associate variables listed in Table 3.1. The selector in the DCS makes the control structure flexible. Hence, it is possible to customize the supervisory control framework by letting some variables be controlled by level 1 PID and letting the other variables be controlled by level 2 MPC or nonlinear MPC (NMPC). Three supervisory-level control schemes are also listed in Table 3.1, including scheme 1, which uses only PID; scheme 2, which uses only MPC; and scheme 3, which uses only NMPC. It should be noted that the level 0 PLC or PID is absolutely required in all cases.

When MATLAB PID Tuner Toolbox is used to tune the PID controllers, the tuning parameters are automatically calculated by adjusting response time and the transient behavior (robust or aggressive). The difference in the performance observed between MPC and NMPC is principally

in the model used in the control algorithm. The linear time-invariant (LTI) state-space model is commonly applied in MPC and is represented as below.

$$\frac{dx}{dt} = Ax + Bu \qquad \text{Eq. 3.24}$$

$$y = Cx + Du \qquad \text{Eq. 3.25}$$

where x is the vector of state variables, u is the vector of model inputs, y is the vector of model outputs, and A, B, C, and D are constant matrices of appropriate dimensions. The MATLAB Linear Analysis Toolbox is used to obtain a linear approximation of the nonlinear plant model at a specified operating point. Then, MATLAB Model Predictive Control Toolbox provides an environment to manually enter tuning parameters including prediction horizon, control horizon, sampling time, and weights. By contrast, it is more challenging to design the NMPC controller because no NMPC templates or toolbox are provided in Simulink. Therefore, an S-function which can call other user-defined functions (.m files) is built, enabling nonlinear models mentioned in section 3.2.1 to be included in the 'fmincon' solver to optimize the objective function as Eq. 3.23.
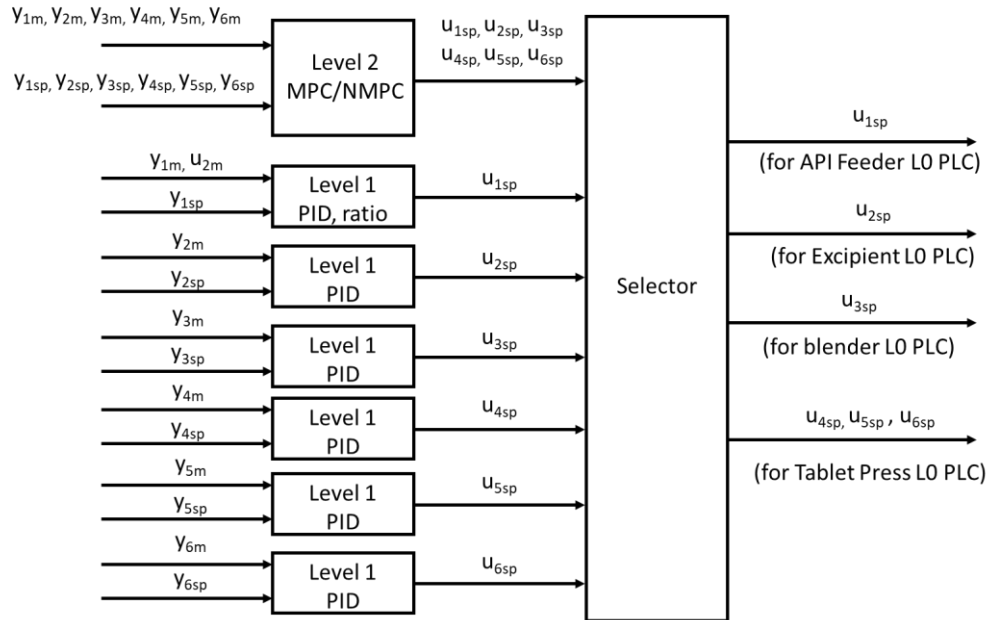
Figure 3.6 Control structure in the supervisory level 1 and level 2 control system

Table 3.1 Process variables and supervisory control schemes

Critical process points	Model output (y) Controlled variables	Model input (u) Manipulated variables	Supervisory scheme1	Supervisory scheme2	Supervisory scheme3
Blender	API Composition (y_1)	API flow rate (u_1)	PID + ratio	MPC	NMPC
	Powder flow (y_2)	Excipient flow (u_2)	PID	MPC	NMPC
	API RSD (y_3)	Blender rotation speed (u_3)	PID	MPC	NMPC
Tablet press	Tablet weight (y_4)	Dosing position (u_4)	PID	MPC	NMPC
	Main compression force (y_5)	Main thickness (u_5)	PID	MPC	NMPC
	Production rate (y_6)	Turret speed (u_6)	PID	MPC	NMPC

3.4   Simulation Results

3.4.1   Control Performance under Risk Scenarios

When API and excipients are delivered by LIW feeders, the weight measurement is crucial for the L0 PLC to adjust the screw rotation speed to maintain the desired mass flow. The sudden change of the powder weight (e.g. refilling) and unexpected events (e.g. powder ratholing, bridging, agglomeration) can cause variations in the mass flow rate. Moreover, the vibration in the feeder caused by the screw rotation can disturb the load cell measurement frequently and result in the calibration error of the LIW feeder itself.

Three control loops are considered: (1) level 0 open loop, (2) level 1 PID closed-loop only using the API composition measurement at the exit of the blender, which is the most common case reported in the literature [2, 47, 48], and (3) level 1 PID closed loop with the measurements of both the API composition and the powder flowrate at the exit of the blender, which is the case to show

the benefits of mass flow sensing. The only distinction between the second case and the third case is the existence of blend flow control, which means that the tablet press is controlled by the same level 1 PID controllers in both cases. Without loss of generality, a calibration error of -20% is introduced in the excipient LIW feeder at t = 300 sec to represent the risk scenario as shown in Figure 3.7. Some metrics are used to quantify the control performance, including integral of time absolute error (ITAE), out-of-specification (OOS) time, duration-to-reject (D2R), and magnitude-to-product (M2P). To be clear, OOS time means the period during which the CQA is not within the tolerance limits. D2R is the length of time that the process requires to smooth out the process disturbance or to reach a new set point for the CQA. M2P describes the maximum deviation in the CQAs from the target setpoint. The lowest values of the above indicators are preferred. The evaluations of control performance in terms of these metrics and based on the API composition and the tablet weight are listed in Table 3.2.

Under the risk scenario of the calibration error in the feeder, the level 0 open control loop fails to maintain the API composition, the powder flow rate, and the tablet weight at the target values. In addition, the tablet press hopper level drops significantly from 50% to 23.2%, which may result in the potential risk of a shortage of powders. By contrast, both level 1 closed control loops can correct the API composition back to the ± 5% tolerance limit and maintain the tablet weight within 0.11% error. Moreover, the closed loop with mass flow sensing exhibits better control performance than the closed loop without mass flow sensing, given M2P of API composition (5.9% < 6.1%) and DR2 of API composition (211 sec < 245 sec). When the API composition is beyond 5% control limits, the OOS materials/products must be diverted. In other words, PID with mass flow sensing will waste approximate 950 tablets over the OOS time of 72 seconds (blue line from t = 337 sec to 445 sec), saving more materials compared to PID without mass flow sensing which produces 1350 wasted tablets in the OOS time of 102 seconds (brown line from t = 380 sec to t = 482 sec).

It should be noted that the change of API composition at the exit of the blender does not affect the tablet weight immediately because of the residence time of the material in the tablet press hopper This is the reason that the tablet weight is affected only after t = 440 sec rather than beginning at t = 300 sec in all cases. The residence time is approximately equal to the powder weight in the tablet

press hopper divided by the production rate of tablets. While D2R and M2P of the tablet weight are almost the same in both closed-loop cases, smaller ITAE of the tablet weight in the case with mass flow sensing denoted fewer variations in the tablet weight. From the viewpoint of hopper level, PID with mass flow sensing keeps the blend flow rate within 5% error and the hopper level within 3.3%, which is obviously better than obtained with PID without mass flow sensing. Therefore, the additional PAT tool for mass flow sensing (e.g. ECVT sensor) can make the control strategy more robust under these risk scenarios.
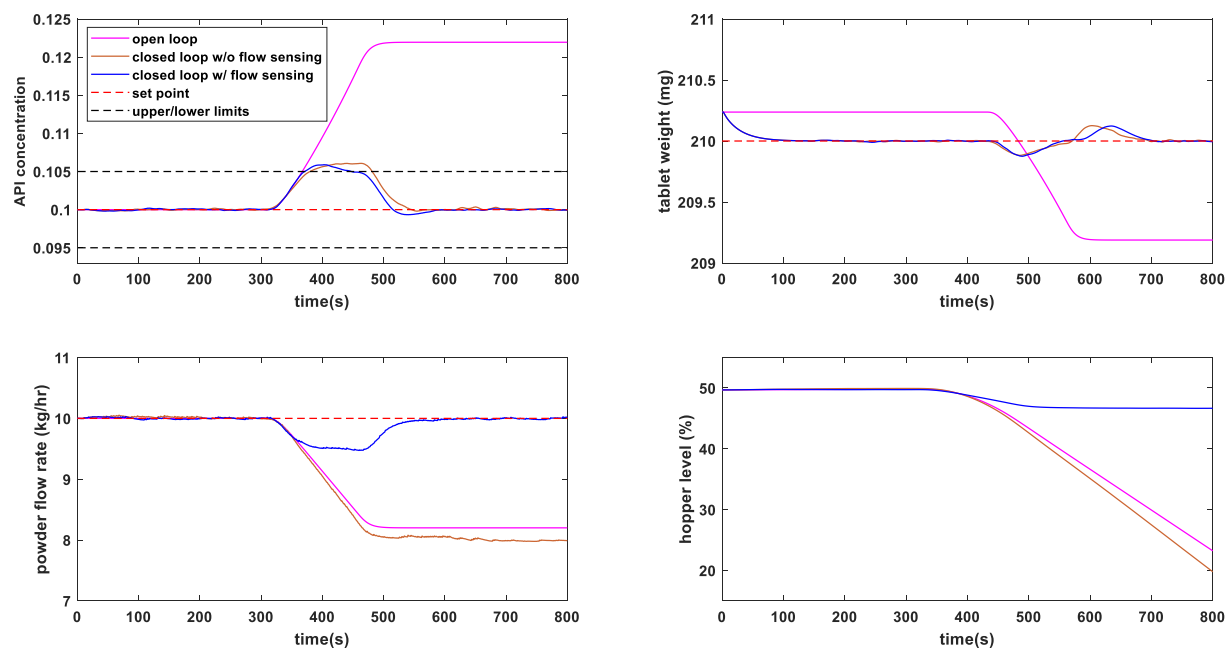
Figure 3.7 Control performance when the calibration error occurs to the LIW feeders

Table 3.2 Performance evaluation based on API composition and tablet weight

CQA	Performance indicators	L0 open loop	L1 closed loop without flow sensing	L1 closed loop with flow sensing
API Comp	OOS time(sec)	Fail	102	72
	D2R (sec)	Fail	245	211
	M2P (%)	22	6.1	5.9
Tablet weight	D2R (sec)	Fail	270	270
	M2P(%)	0.0024	0.11	0.11
	ITAE (sec)	809.3	46.4	44.2

3.4.2 Disturbance Rejection

The capability of disturbance rejection plays a key role in maintaining operations within specification, especially when the system becomes more complex and nonlinear. The ability of level 1 closed-loop control with mass flow sensing for disturbance rejection is shown in Figure 3.8. A sinusoidal disturbance of $0.6 \sin(\pi t / 300)$ kg/hr is added to the powder flow rate at the exit of the blender. The powder flow rate violates the 5% operation limit in the level 0 open-loop control scenario. However, when the level 1 closed-loop control is applied, the disturbances are suppressed and the powder flow rate is maintained within 2.2%. In addition, the controlled powder flowrate reduces the disturbances in the tablet press hopper level as well, which can potentially lower the disturbances in the properties of powders entering the feed frame.
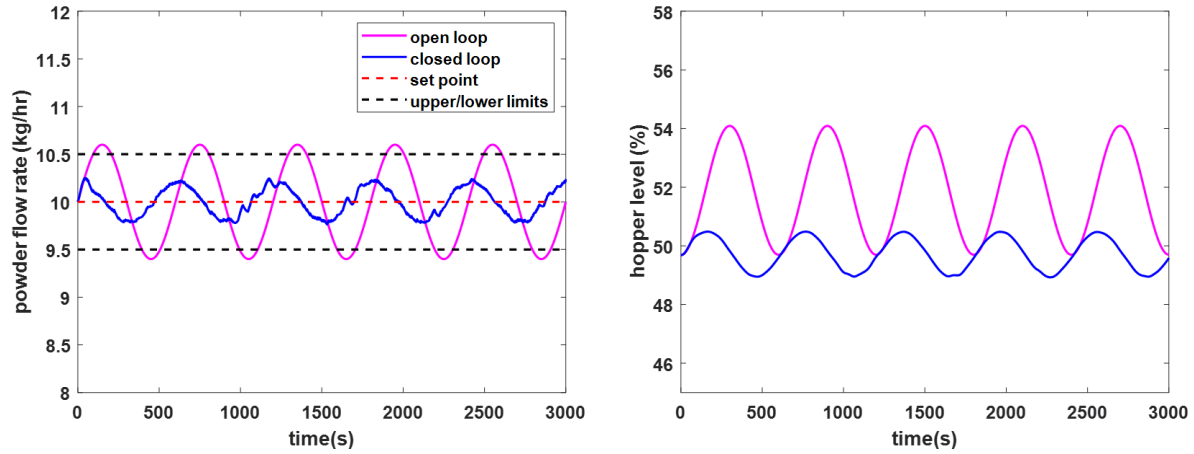
Figure 3.8 Disturbance rejection performance for the closed-loop control with mass flow sensing

The disturbances in tablet weight are in part attributed to the variations in the turret speed, which affects the time of die filling. The comparison of two cases of level 1 closed loop control for adjusting the turret is shown in Figure 3.9. A sinusoidal disturbance of $0.6 \sin(\pi t / 300)$ kg/hr is again imposed on the powder flow rate at the exit of the blender as a disturbance in the hopper level and the set point of the tablet weight is 210 mg in both cases. One case is the level-controlled closed-loop (orange line), which is the most common control strategy employed in continuous direct compression tableting lines in the literature. To maintain the hopper level at the setpoint value 50%, the required frequent changes in the turret speed can lead to variations in the tablet weight (-0.070 ~ +0.080 mg). The other case is the rate-controlled closed-loop (blue line), where the turret speed is altered according to the mass flow measurement of tablets. As the tablet production rate is controlled at 10 kg/hr, less frequent adjustment of the turret speed is required. At the expense of larger variations in the hopper level, the variations in the tablet weight are mitigated (-0.058 ~ 0.043 mg) compared to the level-controlled case.
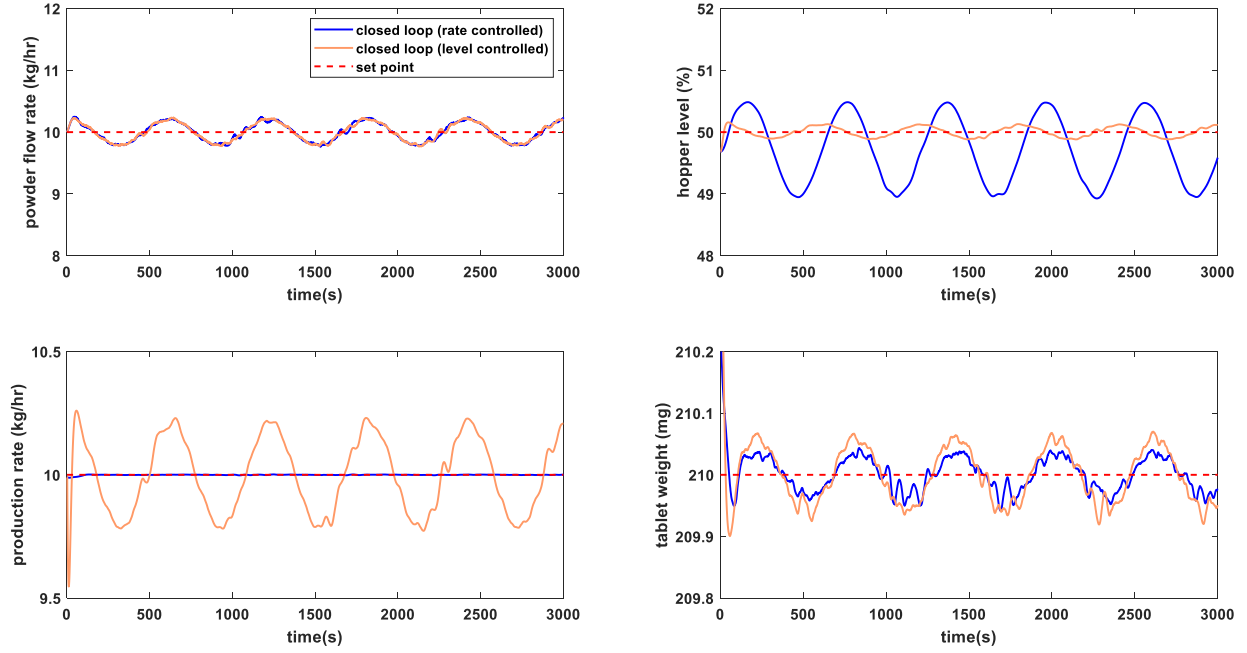
Figure 3.9 Comparison of control performance when the turret speed is adjusted depending on different variables

Following the comparison of the rate-controlled closed loop and the level-controlled closed loop, an interaction analysis for the MIMO system can be further investigated using the relative gain array (RGA) analysis represented by equations below.

$$G(s) = C(sI - A)^{-1}B + D \qquad \text{Eq. 3.26}$$

$$\Lambda = G(s = 0) \odot (G^{-1}(s = 0))^T \qquad \text{Eq. 3.27}$$

where G(s) is the system transfer function matrix. A,B,C, and D are the same matrices in the state-space model in Eq. 3.24 and Eq. 3.25. I is identity matrix. Λ is the RGA. G(s=0) is the steady-state gain matrix. RGA is defined as the ratio of an open loop gain to the same loop gain when the other loops are under perfect control. When the RGA element (i,j) in the ith row and the jth column is close to one, it means that the ith output and the jth input is the optimal control-loop pairing. In other words, values in RGA deviating from one represents an unstable system and high process interaction. Given 6 inputs and 6 outputs in the system, the RGA of 6x6 dimension for the rate-controlled closed loop and the level-controlled closed loop are listed in Table 3.3 and Table 3.4 respectively.

49

Table 3.3 RGA of the process when the tablet production rate is a controlled variable (y6)

	u_1 API flow	u_2 excipient flow	u_3 blender rpm	u_4 dosing position	u_5 main thickness	u_6 turret speed
y_1 API Comp	0.900	0.100	0.000	0.000	0.000	0.000
y_2 powder flow	0.100	0.900	0.000	0.000	0.000	0.000
y_3 API RSD	0.000	0.000	1.000	0.000	0.000	0.000
y_4 tablet weight	0.000	0.000	0.000	0.982	0.000	0.018
y_5 main force	0.000	0.000	0.000	0.000	1.000	0.000
y_6 production rate	0.000	0.000	0.000	0.018	0.000	0.982

Table 3.4 RGA of the process when the hopper level is a controlled variable (y6)

	u_1 API flow	u_2 excipient flow	u_3 blender rpm	u_4 dosing position	u_5 main thickness	u_6 turret speed
y_1 API Comp	3.497	-2.553	0.000	0.092	0.000	-0.036
y_2 powder flow	-0.072	0.178	0.000	0.016	0.000	0.877
y_3 API RSD	-2.426	3.374	0.001	0.001	0.000	0.049
y_4 tablet weight	0.000	0.000	0.000	0.891	0.000	0.109
y_5 main force	0.000	0.000	0.000	0.000	1.000	0.000
y_6 hopper level	3.470	-2.533	0.000	0.091	0.000	-0.036

When the rate-controlled closed loop is applied, the RGA in Table 3.3 indicates that the diagonal pairing should be used because these six diagonal values are close to 1, suggesting that this MIMO system can be decoupled into multiple SISO loops. By contrast, the RGA in Table 3.4 shows higher process interaction (off-diagonal values in the range of 2.4 to 3.5) when the level-controlled closed loop is used. Therefore, controlling the mass flow rate of tablets is more beneficial to the process stability than controlling the hopper level.

3.4.3   Intelligent Diverting Control

Under FDA guidance, diverting out-of-specification materials/tablets is a required step in a continuous process to maintain the quality of final products. The concept of residence time

distribution (RTD) has been proposed as an estimate of the time required for materials advanced into downstream unit operations to be diverted. It has been proposed that the RTD-based control approach is more efficient than the fixed window approach [49].

A new concept, intelligent diverting control (IDC), is proposed here to increase the robustness of the diverting procedure as shown in Figure 3.10. Since it is better to control the turret speed based on the production rate measurement rather than the hopper level as discussed in section 3.4.2, it should be noted that the production rate measurement is missing when the diverting gate of the tablet press is on. A conventional approach is to apply the open-loop control mode to maintain the same value of the turret speed as shown in Figure 3.10a. By contrast, the powder flow rate is incorporated in the IDC concept as shown in Figure 3.10b, because the powder flow rate should be the most similar value with the tablet production rate for the purpose of maintaining the process in a state of control. This strategy enables the closed-loop mode to be employed during the diverting process.
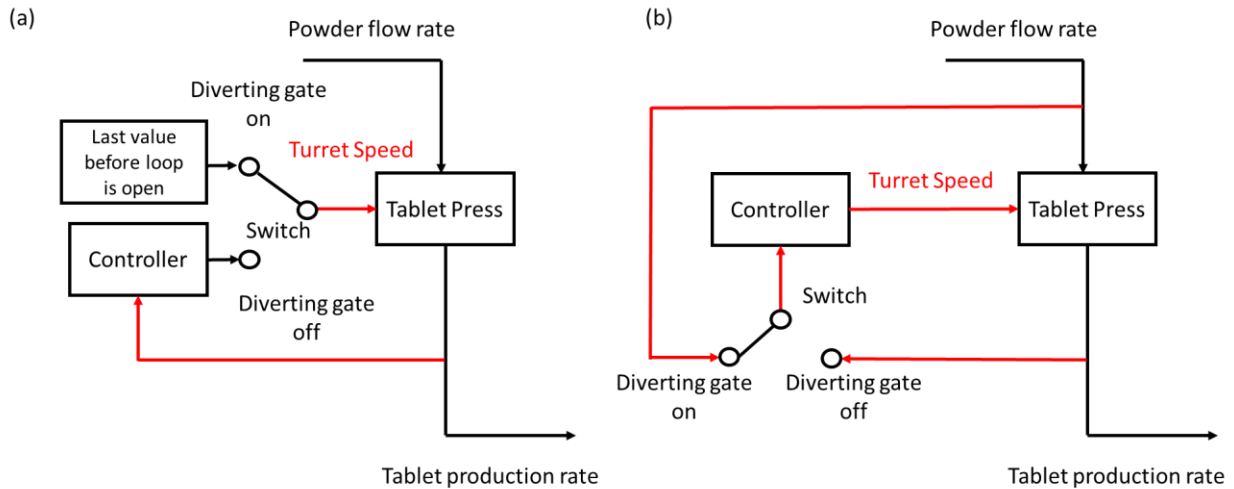
Figure 3.10 Diverting procedures for (a) conventional approach and (b) intelligent diverting control (IDC)

The trigger will open the diverting gate when the measurement error $= |y_{measurement} - y_{setpoint}| / y_{setpoint}$ is larger than tolerance limits, where y is the controlled CQA (e.g. API composition or tablet weight). To investigate the effectiveness of IDC, a disturbance in the bulk density is introduced to the powder in the feed frame at t = 300 sec and the tolerance limits for the tablet weight is set to

51

5% (210 mg ± 10.5 mg) as shown in Figure 3.11. The level 1 PID control is used in both cases including the IDC framework and the conventional method. As evident in Figure 3.11d the diverting gate is on when the 5% tolerance limit is violated from t = 322 sec to t = 365 sec. The rate measurement used in the controller for the turret speed is shown in Figure 3.11c, suggesting that the reading in the IDC framework is not affected by the diverting process with the aid of powder flow sensing but the reading is missing in the conventional approach. When the diverting process ends and the turret speed is manipulated in the closed-loop mode for both cases, the conventional approach suffers from the missing flow measurement and increases the turret speed significantly to compensate for the measurement error as shown in Figure 3.11a, which further causes a large deviation in the hopper level as shown in Figure 3.11b. By contrast, the IDC framework demonstrates improved robustness over the conventional method by resulting in less deviation in the hopper level.
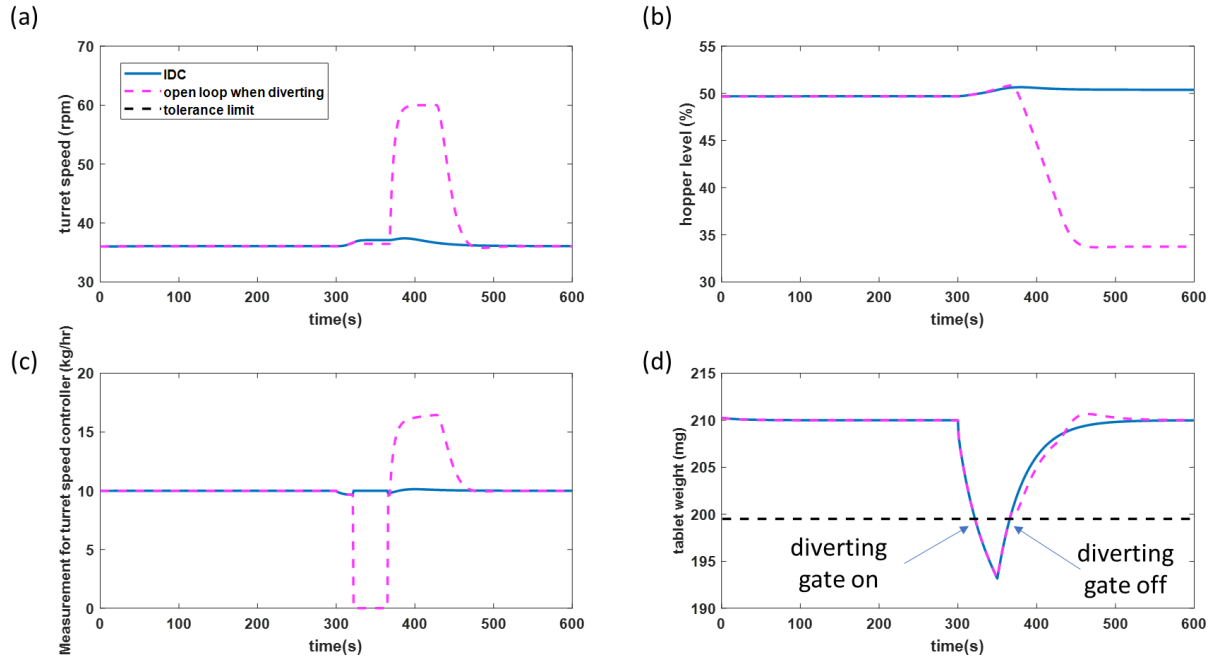

Figure 3.11 Comparison of robustness in IDC and in the conventional approach

3.4.4 Advanced Control Strategies (Level 2 MPC and NMPC)

Higher-level advanced control strategies (e.g. level 2 MPC or level 2 NMPC) can be developed when more measurements (e.g. mass flow sensing) are available and included. More real-time data are beneficial to process understanding and the development of mathematical models, further improving control performance by using active control response to predicted errors. To investigate advanced control strategies, step changes of the API composition and the tablet weight are introduced into three kinds of control schemes as shown in Figure 3.12, including level 1 cascaded PID, level 2 MPC, and level 2 NMPC. The evaluations of control performance are listed in Table 3.5.

Given the rise time and the fall time, defined as the time required for the response to rise or fall from 10% to 90% of the final value, NMPC demonstrates the most efficient capability of setpoint tracking. Moreover, it is observed that larger step change in tablet weight (from 210 mg to 140 mg) can be better handled in NMPC than in MPC (fall time 39 sec < 47 sec), although there is almost no difference of rise time (both 38 sec) in smaller step change (from 175 mg to 210 mg) between MPC and NMPC, as evident from Figure 3.12d. This can be attributed to the fact that the control performance deteriorates as the tablet weight deviates from the nominal value (210 mg) and the plant-model mismatch increases in MPC.

While the powder flow rate and API root mean squared deviation (RSD) can be controlled at their set points by three control schemes as shown in Figure 3.12b and Figure 3.12c, both MPC and NMPC show better control of the main compression force and the production rate compared to cascaded PID as shown in Figure 3.12e and Figure 3.12f. That occurs because the optimization-based level 2 control can determine the appropriate moves for every manipulated variable simultaneously and thus can mitigate the effects of process interactions. Based on M2P and ITAE values, it can be shown that NMPC can reject the disturbances in the main compression force more effectively than MPC, but MPC has better control performance on maintaining production rates compared to NMPC. The results can be explained by the fact that different weights (W_j^y and $W_j^{\Delta u}$) are chosen in the objective function in Eq. 3.23 as well as the fact that NMPC tracks the setpoint of tablet weight more aggressively than MPC. Overall, advanced level 2 control schemes can

provide improved setpoint tracking and disturbance rejection than level 1 PID does, which supports the idea that more process measurements are required to understand the process and implement effective control structures.
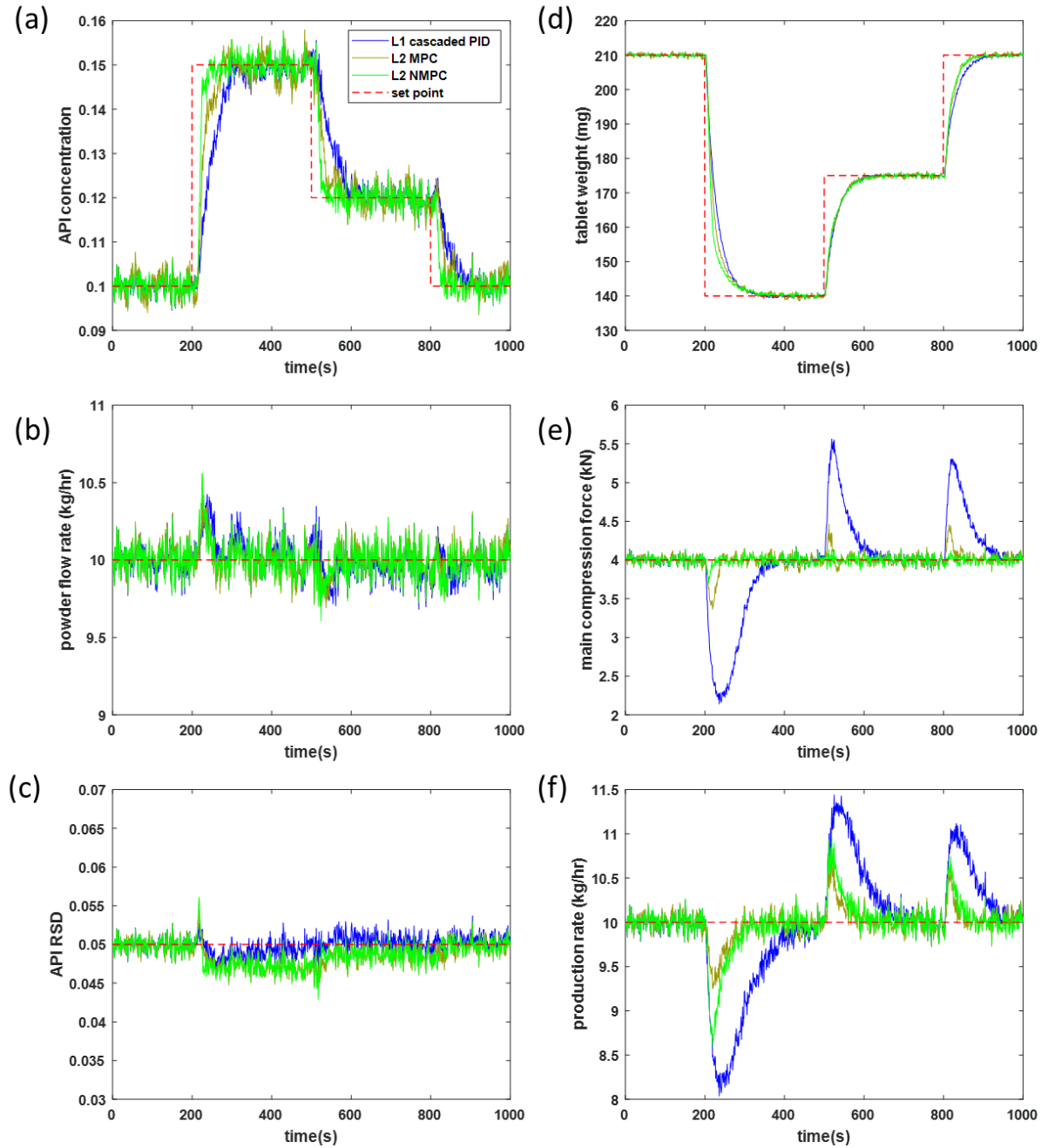

Figure 3.12 Control performance for Level 1 PID, Level 2 MPC and Level 2 NMPC

Table 3.5 Performance evaluations of different control schemes (PID, MPC and NMPC)

Variables	Performance indicators	level 1 PID	level 2 MPC	level 2 NMPC
API Comp	Rise time of large step change (sec)	86	58	26
	Fall time of small step change (sec)	79	38	13
Tablet weight	Fall time of large step change (sec)	55	47	39
	Rise time of small step change (sec)	63	38	38
Main force	ITAE (sec)	37978	8211	5199
	M2P (%)	46.5	15.9	7.6
Production rate	ITAE (sec)	20093	6017	7289
	M2P (%)	19.6	8.5	14.0

3.4.5   Effects of Sampling Time and Measurement Precision

Given that different PAT tools for mass flow sensing (e.g. ECVT sensor, X-ray sensor, and load cell) can have different rates of data acquisition and measurement precision, it is important to know the effects of data sampling. Generally, too large a sampling time can cause aliasing and too small a sampling time can impose burdens on data storage and computing time. To deal with the noise in the raw data, the moving average filter is a common tool to improve measurement precision.

In the simulated process, a setpoint change (from 10 kg/hr to 15 kg/hr) is introduced in the powder flowrate at t = 200 sec, and then another setpoint change (from 15 kg/hr to 10 kg/hr) is introduced at t =600 sec to return the powder flow rate back to the nominal value. Setpoint tracking of powder flow causes variations in the API composition. Therefore, ITAE and M2P of the API composition are used to evaluate the effects of sampling time of mass flow sensing on three different control schemes, as shown in Figure 3.13. It should be noted that ITAE and M2P here are normalized so we can demonstrate the effects of sampling time more clearly. The sampling times for PID, MPC, and NMPC are fixed at 1 sec, 3 sec, and 3 sec respectively. As the sampling time of powder flow is increased, the observations and discussions for three control schemes are described as follows:

(a) For PID, while M2P remains almost the same, ITAE is increasing slightly with 1.04 times variation produced when sampling time is 6 sec. The sampling time does not affect the control performance of the PID controller very much. Consequently it is not necessary to reduce sampling time as much as possible, which is supported by the observation that there is no improvement when sampling time of sensing (0.5 sec) is less than sampling time of PID controller (1 sec)

(b) For MPC, both M2P and ITAE are suddenly increasing when the sampling time is much larger than the sampling time of MPC (3sec), which is supported by 1.80 times ITAE and 1.48 times M2P when sampling time of mass flow sensing is 5sec. It should be noted that the control performance of MPC does not significantly deteriorate when the sampling time of flow sensing (4 sec) is a little larger than the sampling time of MPC (3sec).

(c) For NMPC, both M2P and ITAE are immune to the effects of sampling time. The reason for the immunity to sampling time in NMPC is that there is no model-plant mismatch in the simulation.
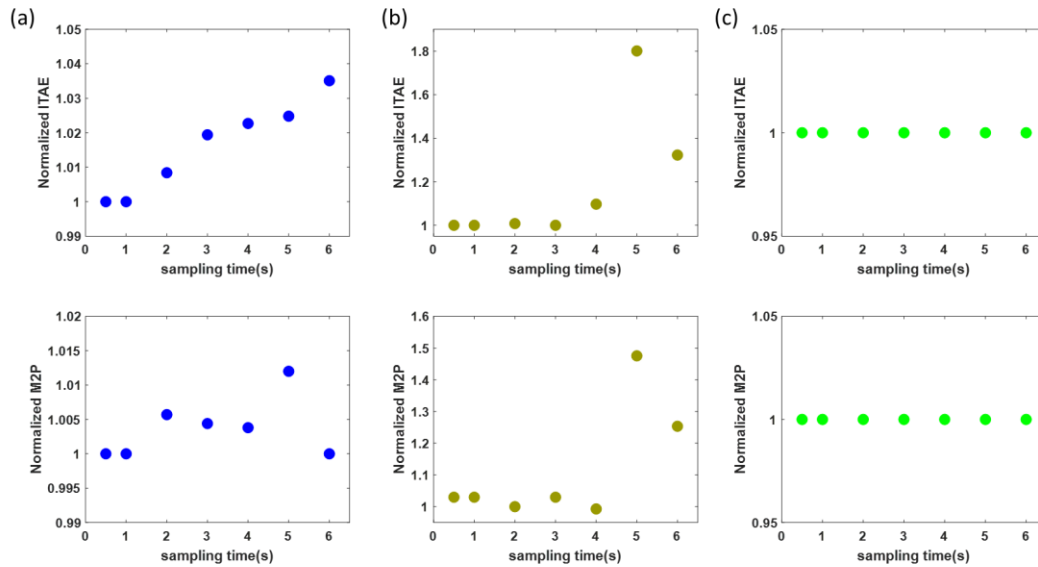

Figure 3.13 Effects of sampling time on different control schemes including (a) level 1 cascaded PID, (b) level 2 MPC and (c) level 2 NMPC

To investigate the effects of the average window size, a similar setting is used. In the simulated process, a setpoint change (from 10 kg/hr to 15 kg/hr) is introduced in the powder flowrate at t = 200 sec, and then another setpoint change (from 15 kg/hr to 10 kg/hr) is introduced at t =600 sec to return the powder flow rate back to the nominal value. In addition, random noise is introduced to the mass flow measurement. The normalized ITAE and normalized M2P of the API when different average window sizes are used are shown in Figure 3.14.

Under PID control in Figure 3.14a and MPC in Figure 3.14b, the raw noise data (frame size = 1) can lead to high ITAE and M2P compared to filtered data. The noise significantly deteriorates the control performance of MPC, as supported by the 1.8 times ITAE and 2.2 times M2P. The window size of 50 frames is the best choice to filter the noise data. Too large a window size can result in adverse effects, with MPC performance much more negatively impacted (1.35 times ITAE) when the window size is too large (≥300 frames) compared to PID performance(1.06 times ITAE). In Figure 3.14c, it can be seen that NMPC is insensitive to the average window size, which can be attributed to no plant-model mismatch in the simulation.
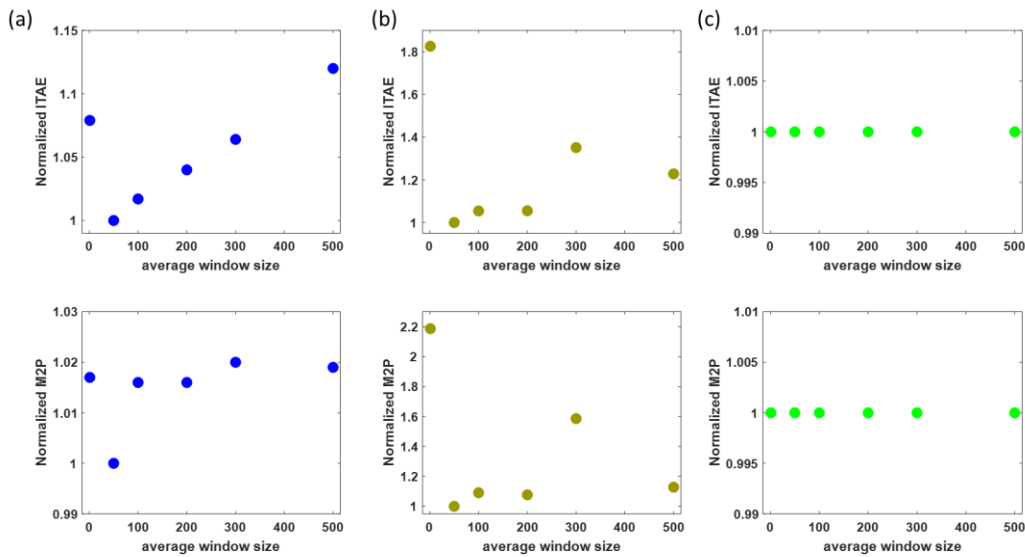

Figure 3.14 Effects of the average window size on different control schemes including (a) level 1 cascaded PID, (b) level 2 MPC and (c) level 2 NMPC

3.5 Conclusions

Under the concept of QbC, robust active control is required to respond to risk scenarios and to reject disturbances in pharmaceutical manufacturing. Flowsheet modeling executed in MATLAB Simulink is used to investigate the applications of mass flow sensing to the plant-wide control system in a continuous direct compaction process, consisting of LIW feeders, a blender, and a tablet press. The three-level hierarchical control structure is investigated in this study, including equipment based level 0 PLC control, level 1 PAT based property feedback control (PID), and level 2 model and optimization based supervisory control (MPC and NMPC).

When the level 1 PID control scheme is used to manipulate the API flowrate and the excipient flow rate, the closed-loop control with both the blend flow measurement and the API composition measurement at the exit of the blender has better control performance than the closed-loop control with only the API composition measurement, as supported by the OOS time, D2R, M2P, and ITAE of CQAs. In addition, the controlled flow rate is beneficial in significantly reducing variations in the hopper level, which is an important buffer inventory and can not be controlled by using only ratio control and the API composition measurement under risk scenarios. While it is common to control the hopper level by adjusting the turret speed, simulation results show that variations in the tablet weight can be mitigated by level 1 PID closed-loop which adjusts the turret speed depending on the tablet production rate instead of the hopper level. Moreover, RGA analysis also indicates that process interaction (value 2.4 – 3.5 in RGA) is stronger when the hopper level is one of the controlled variables, but the system can be approximately decoupled into several SISO pairings (the diagonal values are close to 1 in RGA) when the hopper level is replaced by the production rate. Therefore, it is a better operating strategy to monitor the hopper level rather than to directly control it. Under the conventional procedure of diverting out-of-specification tablets, the measurement of the production rate is lost when the diverting gate is open. When the powder flow rate is also incorporated into the control strategy for adjusting the turret speed, it is evident that the variations in the hopper level can be reduced.

With more PAT measurements and real-time information, the mathematical models followed by process understating can be developed and used for prediction, further enabling high-level

58

advanced control strategies such as level 2 MPC and NMPC. In a MIMO system, model and optimization based level 2 control can deal with the process interaction better than level 1 PID because decoupled SISO systems may fail in a complex and nonlinear system. When the setpoint change is introduced to the API composition and the tablet weight, both MPC and NMPC show the better capability of setpoint tracking and disturbance rejection in the main compression force and production rate.

Given different techniques for mass flow sensing (ECVT sensor, X-ray sensor, and load cell), the effects of sampling time and measurement precision are discussed. A setpoint change of powder flow is introduced and the ITAE of API composition is used to evaluate the effects of mass flow sampling. Increased sampling time and inappropriate window size slightly impact level 1 PID. However, when the sampling time of mass flow sensing is larger than the sampling time of MPC, the control performance deteriorates the most. It is observed that NMPC is insensitive to both sampling time and average window size because there is no model-plant mismatch.

In conclusion, all of the simulation results indicate that mass flow measurements (powder flow and tablet production rate) make the control strategy more robust in handling risk scenarios, rejecting disturbances, providing a better candidate in RGA for decoupled pairings, and reducing variations during the diverting process. Higher-level advanced control strategies can also be implemented in a plant-wide MIMO system such as a direct compaction line when mass flow rates are measured.

4. EXPERIMENTAL IMPLEMENTATION

4.1 Continuous Direct Compaction Line

As discussed in Section 3.2 (Process Description), the continuous direct compaction line of the pilot plant at Purdue University consists of two Schenck AccuRate PureFeed® AP-300 loss-in-weight feeders (LIW) (Figure 4.1a), one each for API and excipient. The API and excipients are dispensed at target flow rates from respective LIW feeders and fed into Gericke GCM-250 continuous blender (Figure 4.1b). Upon exiting the blender, the blend is transferred by gravity flow to the commercial-scale tablet press Natoli NP-400, which has 22 stations with concave-head punches (Figure 4.1d). Inside the chamber of the tablet press, the NIR probes of Innopharma Multieye$_2$ spectrophotometer can be located both in the hopper and the feed frame to measure API concentration (Figure 4.1c).
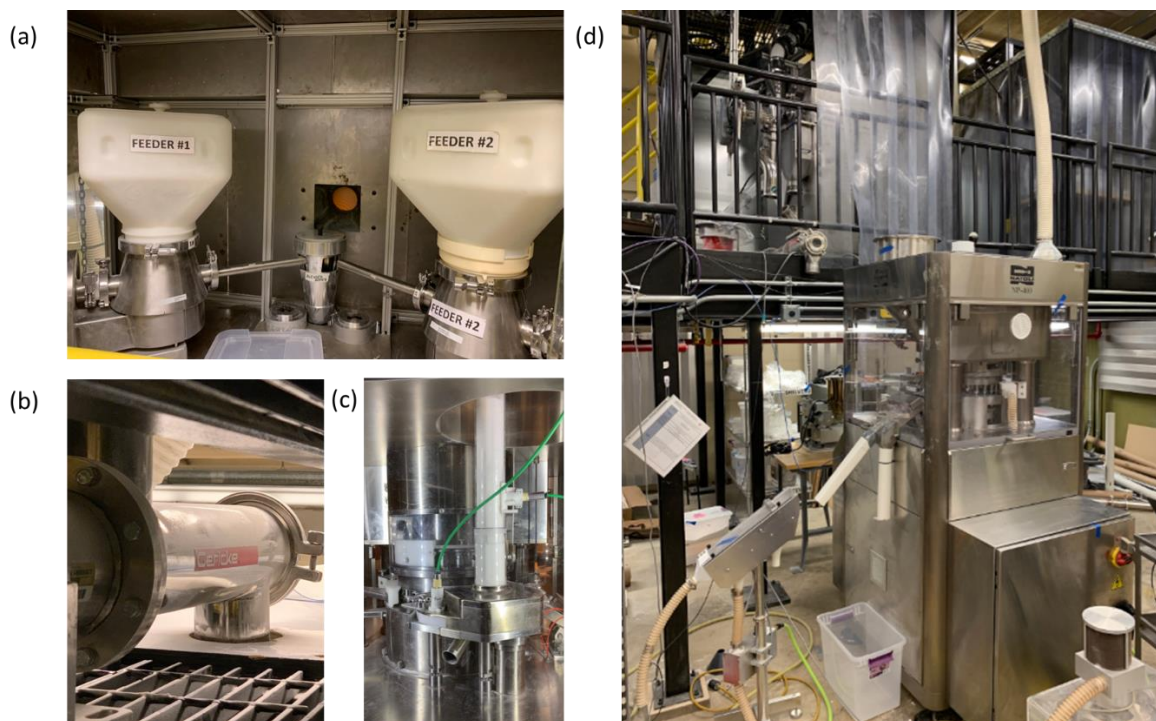

Figure 4.1 Unit operations in the direct compaction line including (a) loss-in-weight feeders, (b) continuous blender, (c) hopper associated with the tablet press, and (d) tablet press

Continuous blending is the first step in the continuous tablet manufacturing line in which API is mixed with excipients to meet the required API concentration and content uniformity. Given that it is hard to correct the API concentration in the downstream unit operations (e.g. tablet press in a direct compaction line, and roller compactor in a dry granulation line), the feeding-blending subsystem has to be properly controlled. Therefore, an experimental setup incorporating both the ECVT sensor (Figure 4.2b) and the NIR sensor (Figure 4.2c) was used to implement sensor measurements within the distributed control system (DCS) DeltaV. Upon exiting the blender, the blended powder flows by gravity into a concentric reducer which was connected to the 1 inch PTFE pipe as shown in Figure 4.2a, and passes through the ECVT sensor and by the NIR sensor. The mass flow measurement from an independent Mettler-Toledo ME 4001E weighing scale was used to provide the reference mass flow rate in these experiments.
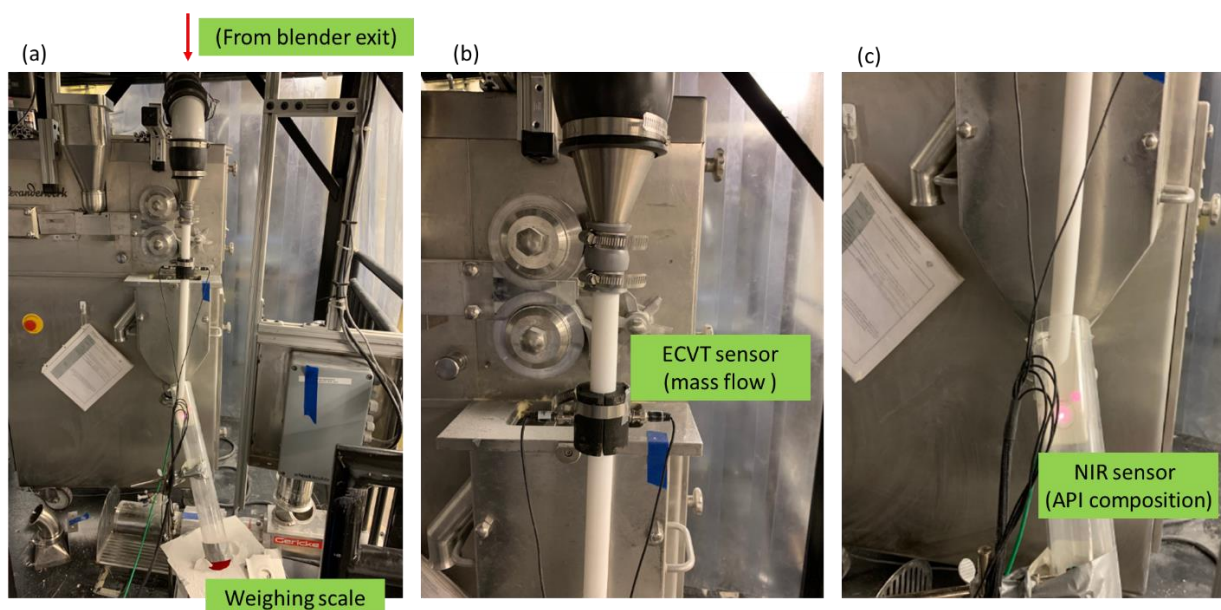

Figure 4.2 Experimental setup for the feeding-blending subsystem

4.2 Experimental Results

API composition is a required measurement for any level 1 or level 2 control structure. In these experiments that composition is obtained using NIR spectroscopy. With the accurate API composition measurement, the powder flow rate control in a plant-wide system can be more robust. The NIR spectrum obtained was converted to a composition value by means of a partial least squares (PLS) regression model. Dynamic samples from the feeding-blending system (8%, 10%, 12%, 14%, 16% API) at 10 kg/hr were used to generate the necessary spectra and to build the PLS model, where 8% means 0.8 kg/hr API and 9.2 kg/hr excipients and so on. The results indicate that the PLS model operating on the NIR measurements was able to detect the concentration difference between 10% API static sample and 14% API static sample, and average measurement errors over 2 minutes were (11.8-10)/10 = 18% and (13.3-14)/14 = -5% as shown in Figure 4.3a. When the NIR sensor was used to measure dynamic powder flow, the API composition of a blend with 10 % API flowing at 10 kg/hr was predicted to be 10.98 % from t = 1:00 to t = 2:30, with the average error of 9.8% as shown in Figure 4.3b. However, when the API composition was increased to 14 % (excipient flow was decreased from 9 kg/hr to 8.6 kg/hr, and API flow was increased from 1kg/hr to 1.4 kg/hr), the NIR sensor failed to detect the concentration change. Even when the powder flow stopped at t=7:30, the API composition still approximately maintained at 10.8%. These two results can be attributed to fouling caused by the powder accumulated in the printed holder for the NIR probe as shown in Figure 4.4
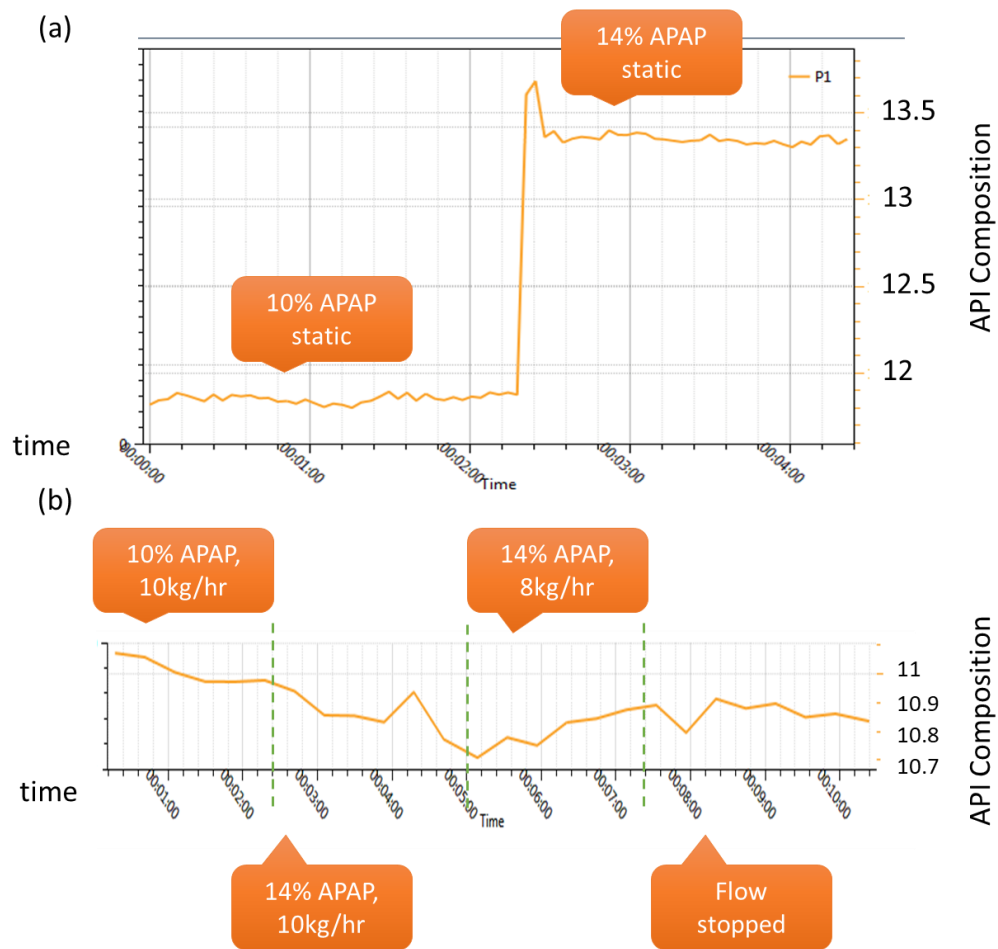
Figure 4.3 API composition measurement when the powder is (a) static or (b) dynamic
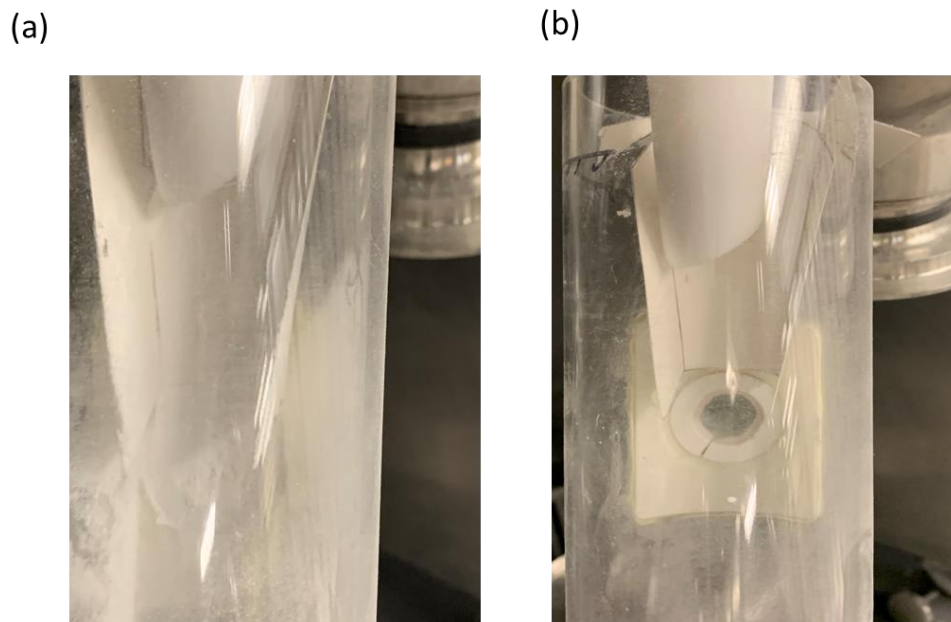
Figure 4.4 NIR probe holder (a) with powder fouling and (b) without fouling

Given some modifications are required in the NIR holder design, an experiment was conducted to demonstrate that the mass flow sensing can increase the control robustness before implementing both API composition measurement and mass flow measurement into the feedback control loop. When the excipient blend (MCC200 + 0.2% MgSt) was delivered at 9 kg/hr as shown in Figure 4.5a, the blender rotation speed was adjusted to emulate some disturbances at the exit of the blender as shown in Figure 4.5b. When the blender rotation speed was adjusted from 200 rpm to 100 rpm at t = 180 sec, the powder flow rate was decreased accordingly then returned back to 9 kg/hr at t = 250 sec as shown in Figure 4.5c. Other step changes of blender rotation speed were introduced at t = 300 sec and t = 420 sec, which both led to disturbances in the powder flow rate. While the LIW feeder of course could not capture variations in the flow rates, the ECVT sensor did measure these changes caused by powder holdup and residence time in the blender. The average error of the ECVT sensor was – 13.1%, which was computed by comparing each point relative to the weighing scale at the same point.
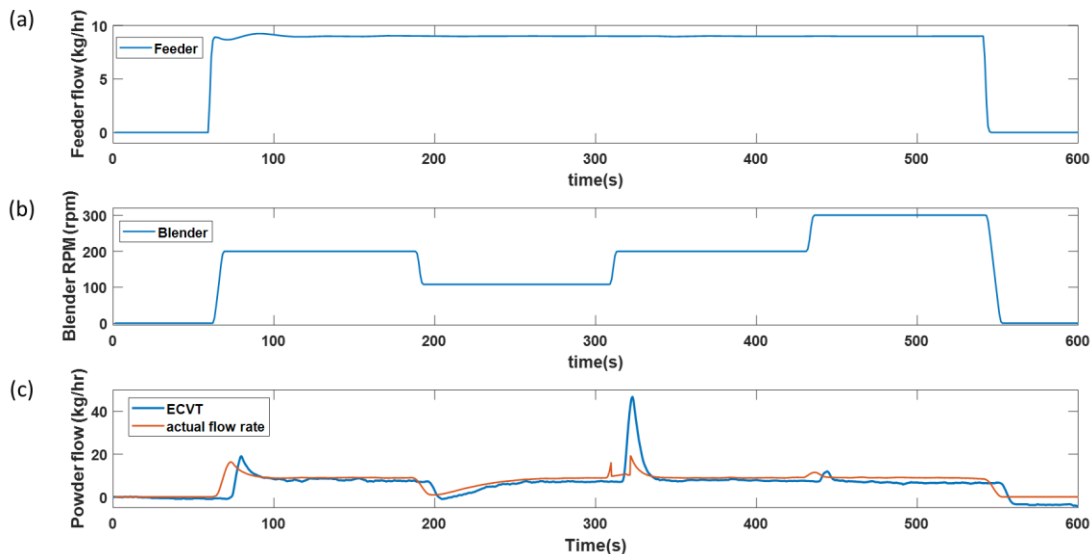
Figure 4.5 Flow rate monitoring in the feeding blending system including (a) excipient flow rate (b) blender rotation speed, and (c) flow rate at the exit of blender

4.3   Conclusions

To control the mass flow rate of blended powder, an accurate API composition measurement is required to complement the mass flow measurement for implementing level 1 or level 2 supervisory plant-wide control. A partial least squares (PLS) regression model for the NIR spectroscopy-based sensor was used to predict the API composition. The results indicated that the NIR sensor and the PLS model can detect API composition of static samples. However, the NIR probe holder must be redesigned to mitigate the effects of fouling, in order to enable accurate real-time API concentration measurements. The ECVT sensor has already been implemented in the exit of the blender. By adjusting the blender rotation speed to emulate disturbances in the blender, it is observed that the ECVT sensor can capture the flow dynamics at the exit of the blender, which is impossible to be measured by LIW feeders. Therefore, the mass flow measurements from the ECVT sensor definitely will make the control structure more robust by rejecting measured disturbances.

5. FUTURE WORK

In the future, the mass flow measurements of the ECVT sensor will be sent to the DCS system DeltaV via OPC Unified Architecture (OPCUA) server in real-time. In addition, when the reliable real-time API composition measurement is obtained, the comparative performance of the closed-loop control studies with both mass flow measurements and API composition measurements and the one with only API composition measurements will be carried out. Moreover, the entire direct compaction process will be operated in integrated fashion via the Level 1 and 2 closed-loop control structures.

More measurement redundancy is beneficial to process understanding and mathematical model development. The mass flow rate can be applied to estimate unmeasured variables such as blender holdup, which plays a key role in determining residence time and content uniformity. Hence, state estimation will be investigated in the future. State estimation is a useful technique for process monitoring, control, and real-time optimization. It not only provides estimates of unmeasured variables, but also filters the measured variables by using the mathematical models as optimization constraints. Compared to the direct measurements applied in the closed-loop control, the state estimates can make the controller more robust by eliminating the effects of gross errors or bias, both of which are very common problems arising in the use of on-line sensors. For nonlinear dynamic systems in continuous pharmaceutical manufacturing, moving horizon estimation (MHE) is a well-known strategy for constrained state estimation. The basic theory in MHE is to estimate the current state of the process using only the last L states and sensor measurements directly, where L is the horizon length.

Process understanding, which relies on the measurements of material properties and real-time process data, is a must for developing advanced level 2 NMPC control schemes. For linear MPC, there exists commercial software like DeltaV which facilitates the construction of the linear state-space model automatically by using perturbations in the input and output variables of the real plant. By contrast, although NMPC usually offers better control performance than MPC, plant-model mismatch can deteriorate the control performance of the NMPC control scheme more easily in the

real plant compared to MPC because of the uncertainty in the nonlinear mathematical models and their parameters. Therefore, the mass flow and other on-line measurements will be used to demonstrate on the real pilot plant how plant-model mismatch can be mitigated via real-time process data and as-needed updating of parameters in the NMPC models.

REFERENCES

[1]   Q. Su *et al.*, "A perspective on Quality-by-Control (QbC) in pharmaceutical continuous manufacturing," *Computers & Chemical Engineering,* vol. 125, pp. 216-231, 2019.

[2]   C. L. Burcham, A. J. Florence, and M. D. Johnson, "Continuous manufacturing in pharmaceutical process development and manufacturing," *Annual review of chemical and biomolecular engineering,* vol. 9, pp. 253-281, 2018.

[3]   M. Ierapetritou, F. Muzzio, and G. Reklaitis, "Perspectives on the continuous manufacturing of powder-based pharmaceutical processes," *AIChE Journal,* vol. 62, no. 6, pp. 1846-1862, 2016.

[4]   S. L. Lee *et al.*, "Modernizing Pharmaceutical Manufacturing: from Batch to Continuous Production," *Journal of Pharmaceutical Innovation,* journal article vol. 10, no. 3, pp. 191-199, September 01 2015.

[5]   H. Leuenberger, "New trends in the production of pharmaceutical granules: batch versus continuous processing," *European journal of pharmaceutics and biopharmaceutics,* vol. 52, no. 3, pp. 289-296, 2001.

[6]   N. Pagliarulo, "Pharma's slow embrace of continuous manufacturing," 2018.

[7]   P. Inc., "U.S. FDA Approves DAURISMO™ (glasdegib) for Adult Patients with Newly-Diagnosed Acute Myeloid Leukemia (AML) for Whom Intensive Chemotherapy is Not an Option," 2018.

[8]   L. D. Belder, *IFPAC Presentation,* 2019.

[9]   R. Lakerveld, B. Benyahia, R. D. Braatz, and P. I. Barton, "Model-based design of a plant-wide control strategy for a continuous pharmaceutical plant," *AIChE Journal,* vol. 59, no. 10, pp. 3671-3685, 2013.

[10]   Y. Yan, "Mass flow measurement of bulk solids in pneumatic pipelines," *Measurement Science and Technology,* vol. 7, no. 12, p. 1687, 1996.

[11]   I. Barratt, Y. Yan, B. Byrne, and M. Bradley, "Mass flow measurement of pneumatically conveyed solids using radiometric sensors," *Flow Measurement and Instrumentation,* vol. 11, no. 3, pp. 223-235, 2000.

[12]   S. Ganesh, R. Troscinski, N. Schmall, J. Lim, Z. Nagy, and G. Reklaitis, "Application of X-ray sensors for in-line and noninvasive monitoring of mass flow rate in continuous tablet manufacturing," *Journal of pharmaceutical sciences,* vol. 106, no. 12, pp. 3591-3603, 2017.

[13]   F. Kumhála, V. Prošek, and J. Blahovec, "Capacitive throughput sensor for sugar beets and potatoes," *Biosystems engineering,* vol. 102, no. 1, pp. 36-43, 2009.

[14]   A. Wang, Q. Marashdeh, F. Teixeira, and L.-S. Fan, "Applications of capacitance tomography in gas–solid fluidized bed systems," in *Industrial Tomography*: Elsevier, 2015, pp. 529-549.

[15]   J. Li, D. Bi, Q. Jiang, H. Wang, and C. Xu, "Online monitoring and characterization of dense phase pneumatically conveyed coal particles on a pilot gasifier by electrostatic-capacitance-integrated instrumentation system," *Measurement,* vol. 125, pp. 1-10, 2018.

[16]   A. J. Jaworski and T. Dyakowski, "Application of electrical capacitance tomography for measurement of gas-solids flow characteristics in a pneumatic conveying system," *Measurement Science and Technology,* vol. 12, no. 8, p. 1109, 2001.

[17]   S. M. Rao, K. Zhu, C.-H. Wang, and S. Sundaresan, "Electrical capacitance tomography measurements on the pneumatic conveying of solids," *Industrial & Engineering Chemistry Research,* vol. 40, no. 20, pp. 4216-4226, 2001.

[18]   X. Guo, Z. Dai, X. Gong, and Z. Yu, "Application of a capacitance solid mass flow meter in a dense phase pneumatic conveying system of pulverized coal," in *AIP Conference Proceedings*, 2007, vol. 914, no. 1: AIP, pp. 320-327.

[19]   J. Li, M. Kong, C. Xu, S. Wang, and Y. Fan, "An Integrated instrumentation system for velocity, concentration and mass flow rate measurement of solid particles based on electrostatic and capacitance sensors," *Sensors,* vol. 15, no. 12, pp. 31023-31035, 2015.

[20]   K. Ogata, K. Funatsu, and Y. Tomita, "Experimental investigation of a free falling powder jet and the air entrainment," *Powder technology,* vol. 115, no. 1, pp. 90-95, 2001.

[21]   G. Újvári, J. F. Kok, G. Varga, and J. Kovács, "The physics of wind-blown loess: Implications for grain size proxy interpretations in Quaternary paleoclimate studies," *Earth-Science Reviews,* vol. 154, pp. 247-278, 2016.

[22]   Y. Pu, M. Mazumder, and C. Cooney, "Effects of electrostatic charging on pharmaceutical powder blending homogeneity," *Journal of pharmaceutical sciences,* vol. 98, no. 7, pp. 2412-2421, 2009.

[23]   S. Naik, "Experiment and Discrete Element Based Modeling of Granular Flow: Tribocharging and Particle Size Reduction in Pharmaceutical Manufacturing," 2014.

[24]   C. Hubert, P. Lebrun, S. Houari, E. Ziemons, E. Rozet, and P. Hubert, "Improvement of a stability-indicating method by Quality-by-Design versus Quality-by-Testing: A case of a learning process," *Journal of pharmaceutical and biomedical analysis,* vol. 88, pp. 401-409, 2014.

[25]   F. J. Muzzio, P. Robinson, C. Wightman, and D. Brone, "Sampling practices in powder blending," *International journal of pharmaceutics,* vol. 155, no. 2, pp. 153-178, 1997.

[26]   Z. K. Nagy and R. D. Braatz, "Robust nonlinear model predictive control of batch processes," *AIChE Journal,* vol. 49, no. 7, pp. 1776-1786, 2003.

[27]   I. FDA, "Q9 quality risk management," *ICH Harmon Tripart Guidel.,* 2006.

[28]   U. FDA, "US Guidance for Industry: Q8 (2) Pharmaceutical Development Maryland," *Food and Drug Administration,* 2009.

[29]   FDA/ICH, "Q10. Pharmaceutical Quality System. Draft Consensus Guideline," 2007.

[30]   R. Ogilvie, "ICH Q11: Development and manufacture of drug substance," *ICH Quality Guidelines: An Implementation Guide,* pp. 639-665, 2017.

[31]   X. Y. Lawrence *et al.*, "Understanding pharmaceutical quality by design," *The AAPS journal,* vol. 16, no. 4, pp. 771-783, 2014.

[32]   R. Singh, A. Sahay, F. Muzzio, M. Ierapetritou, and R. Ramachandran, "A systematic framework for onsite design and implementation of a control system in a continuous tablet manufacturing process," *Computers & chemical engineering,* vol. 66, pp. 186-200, 2014.

[33]   A. Bhaskar, F. N. Barros, and R. Singh, "Development and implementation of an advanced model predictive control system into continuous pharmaceutical tablet compaction process," *International Journal of Pharmaceutics,* vol. 534, no. 1-2, pp. 159-178, 2017.

[34]   S.-H. Hsu, G. V. Reklaitis, and V. Venkatasubramania, "Modeling and control of roller compaction for pharmaceutical manufacturing," *Journal of Pharmaceutical Innovation,* vol. 5, no. 1-2, pp. 24-36, 2010.

[35] S.-H. Hsu, G. V. Reklaitis, and V. Venkatasubramanian, "Modeling and control of roller compaction for pharmaceutical manufacturing. Part I: Process dynamics and control framework," *Journal of Pharmaceutical Innovation,* vol. 5, no. 1-2, pp. 14-23, 2010.

[36] E. Içten, G. V. Reklaitis, and Z. K. Nagy, "Advanced control for the continuous dropwise additive manufacturing of pharmaceutical products," in *Computer Aided Chemical Engineering*, vol. 41: Elsevier, 2018, pp. 379-401.

[37] L. Hirshfield, E. Içten, A. Giridhar, Z. K. Nagy, and G. V. Reklaitis, "Real-time process management strategy for dropwise additive manufacturing of pharmaceutical products," *Journal of Pharmaceutical Innovation,* vol. 10, no. 2, pp. 140-155, 2015.

[38] E. Simone, W. Zhang, and Z. K. Nagy, "Application of process analytical technology-based feedback control strategies to improve purity and size distribution in biopharmaceutical crystallization," *Crystal Growth & Design,* vol. 15, no. 6, pp. 2908-2919, 2015.

[39] Y. Yang, L. Song, and Z. K. Nagy, "Automated direct nucleation control in continuous mixed suspension mixed product removal cooling crystallization," *Crystal Growth & Design,* vol. 15, no. 12, pp. 5839-5848, 2015.

[40] R. Singh, A. Sahay, K. M. Karry, F. Muzzio, M. Ierapetritou, and R. Ramachandran, "Implementation of an advanced hybrid MPC–PID control system using PAT tools into a direct compaction continuous pharmaceutical tablet manufacturing pilot plant," *International journal of pharmaceutics,* vol. 473, no. 1-2, pp. 38-54, 2014.

[41] R. Singh, M. Ierapetritou, and R. Ramachandran, "An engineering study on the enhanced control and operation of continuous manufacturing of pharmaceutical tablets via roller compaction," *International journal of pharmaceutics,* vol. 438, no. 1-2, pp. 307-326, 2012.

[42] R. Singh, A. D. Román-Ospino, R. J. Romañach, M. Ierapetritou, and R. Ramachandran, "Real time monitoring of powder blend bulk density for coupled feed-forward/feed-back control of a continuous direct compaction tablet manufacturing process," *International journal of pharmaceutics,* vol. 495, no. 1, pp. 612-625, 2015.

[43] G. Tian, A. Koolivand, N. S. Arden, S. Lee, and T. F. O'Connor, "Quality risk assessment and mitigation of pharmaceutical continuous manufacturing using flowsheet modeling approach," *Computers & Chemical Engineering,* vol. 129, p. 106508, 2019.

[44] P. M. Portillo, F. J. Muzzio, and M. G. Ierapetritou, "Using compartment modeling to investigate mixing behavior of a continuous mixer," *Journal of Pharmaceutical Innovation,* vol. 3, no. 3, pp. 161-174, 2008.

[45] Q. Su, M. Moreno, A. Giridhar, G. V. Reklaitis, and Z. K. Nagy, "A systematic framework for process control design and risk analysis in continuous pharmaceutical solid-dosage manufacturing," *Journal of Pharmaceutical Innovation,* vol. 12, no. 4, pp. 327-346, 2017.

[46] Q. Su, Y. Bommireddy, M. Gonzalez, G. V. Reklaitis, and Z. K. Nagy, "Variation and risk analysis in tablet press control for continuous manufacturing of solid dosage via direct compaction," in *Computer Aided Chemical Engineering*, vol. 44: Elsevier, 2018, pp. 679-684.

[47] R. Singh, M. Ierapetritou, and R. Ramachandran, "System-wide hybrid MPC–PID control of a continuous pharmaceutical tablet manufacturing process via direct compaction," *European Journal of Pharmaceutics and Biopharmaceutics,* vol. 85, no. 3, pp. 1164-1182, 2013.

[48] M. Kirchengast *et al.*, "Ensuring tablet quality via model-based control of a continuous direct compaction process," *International journal of pharmaceutics,* vol. 567, p. 118457, 2019.

[49] A. Bhaskar and R. Singh, "Residence time distribution (RTD)-based control system for continuous pharmaceutical manufacturing process," *Journal of Pharmaceutical Innovation,* vol. 14, no. 4, pp. 316-331, 2019.